CRYOSMOS

WP900
Conclusions and Recommendations

Final Report

Version 1.0
July 17, 2017

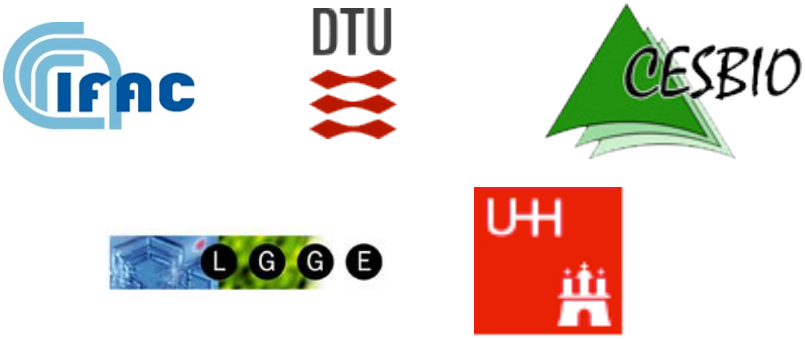

This page is intentionally left blank

<table>
<tr><td colspan="4">ESA STUDY CONTRACT REPORT</td></tr>
<tr><td>ESRIN Contract No:

4000112262/14/I-NB</td><td colspan="2">Subject:

CryoSMOS
Support To Science Elements SMOS+Cryosphere</td><td>Contractor:
IFAC</td></tr>
<tr><td>ESA CR ( )No:</td><td>Star Code:</td><td>No of volumes: 1
This is volume no: 1</td><td>Contractor’s Ref:
Final Report</td></tr>
<tr><td colspan="4">ABSTRACT:
This document is the Final Report (FR) of the study CryoSMOS - Support To Science Elements SMOS+Cryosphere (ESRIN Contract No. 4000112262/14/I-NB). The topic of WP900 is to synthesize all of the findings and work of WP200 – WP800. Conclusions on the work performed in the contract will be elaborated. The report will highlight the key findings and it will include recommendations and outline future work. The key findings will additionally outline the limitations of the novel SMOS products and theirs impact on Cryosphere science.</td></tr>
<tr><td colspan="4">The work described in this report was done under ESA Contract. Responsibility for the contents resides in the author or organisation that prepared it.</td></tr>
<tr><td colspan="4">PREPARED BY:
G. Macelloni, F.Montomoli, M. Brogioni, (IFAC), N. Skou, S. S. Kristensen, R. Forsberg (DTU), M. Leduc-Leballeur, G. Picard (LGGE), L. Kaleschke, A. Wernecke (UHAM), A. Mialon (CESBIO)</td></tr>
<tr><td colspan="2">ESA STUDY MANAGER:
Ola Grabak</td><td colspan="2">ESA BUDGET HEADING</td></tr>
</table>

This page is intentionally left blank

DOCUMENT CHANGE LOG

Issue/ Revision	Date	Observations
1/0	17/07/2017	First issue

This page is intentionally left blank

TABLE OF CONTENTS

This page is intentionally left blank

1 Purpose and structure of document

1.1 Purpose

The CryoSMOS project aims to perform the tasks within the activity SMOS+Cryosphere. This activity is part of the Support To Science Element (STSE), an element of the ESA's Earth Observation Envelope Program (EOEP-4) aiming to reinforce the scientific component of the ESA Living Planet Programme. STSE represents a pathfinder for science and innovation in Earth Observation (EO), providing a flexible mechanism to address the scientific needs and requirements of the Earth system science community in terms of novel observations, new algorithms and products and innovative Earth science results.

This document is the Final Report (FR) for the CryoSMOS project. Its propose is to recall the initial context and project specifications, to compile a synthesis of key results and conclusions of the work performed in the contract and to suggest recommendations and future work directions. The Final Report summarizes in a single and uniform document the work performed in the project. Details of the performed activities are contained in the project's deliverables.

1.2 Document Structure

The structure of the document is the following (and summarized in Table 1-1 against WPs):

- Section 2 – Initial context and summary of the CryoSMOS project
- Section 3 – Synthesis of key results of each case studies
- Section 4 – Conclusion and Recommendations
- Section 5 – References

Table 1-1 - Structure of document against subtasks of the work package

WP	Subtask	Section(s) in document	Main contributors
900	1	1, 2	All
900	1	3.1	IFAC
900	1	3.2	DTU
900	1	3.3	UH
900	1	3.4	LGGE
900	1	4	All

1.3 Definitions and Acronyms

Table 1-2 lists the acronyms and abbreviations used within this documents.

Table 1-2 - Acronyms and abbreviations

Acronym	Meaning
AMSR-E	Advanced Microwave Scanning Radiometer for EO
AMSR-2	Advanced Microwave Scanning Radiometer
AMSU	Advanced Microwave Sounding Unit
CEOS-WGCV	Committee on Earth Observation Satellites-Working Group Calibration and Validation
CESBIO	Centre d'Etudes Spatiales de la BIOsphère
CSCR	Case Studies Consolidation Report
DMRT	Dense Media Radiative Transfer model
DTU	Danish Technical University
ECV	Essential Climate Variables
EM	ElectroMagnetic
EO	Earth Observation
EOEP	Earth Observation Envelope Program
EPICA	European Project for Ice Coring in Antarctica
ESA	European Space Agency
GOCE	Gravity field and steady-state Ocean Circulation Explorer
IFAC	Istituto di Fisica Applicata “N.Carrara”
IR	InfraRed
ITT	Invitation To Tender
LGGE	Laboratoire de Glaciologie et Géophysique de l’Environnement
MODIS	Moderate Resolution Imaging Spectroradiometer
MIRAS	Microwave Imaging Radiometer by Aperture Synthesis
ML	Multi-Layer
NIR	Noise Injection Radiometers
NASA	National Aeronautic and Space Administration

QCA-CP	Quasi Crystalline Approximation with Coherent Potential
RB	Requirement Baseline report
SMAP	Soil Moisture Active and Passive mission
SMOS	Soil Moisture Ocean Salinity mission
SoW	Statement Of Work
SSM/I	Special Sensor Microwave Imager
STSE	Support To Science Elements
TB	Brightness Temperature
UHAM	University of Hamburg
WALOMIS	Wave Approach for LOw-frequency MIcrowave emission in Snow
WP	Work Package

1.4 Reference documents

All the references to scientific works cited in the present report are reported in section References. Hereinafter are listed some general management documents referred in the present report:

[RD.1] Project Statement of Works
[RD.2] CryoSMOS project proposal
[RD.3] D1 - Requirement Baseline report (RB)
[RD.4] D2 - Case Studies Consolidation report (CSC)
[RD.5] D3 - Dataset
[RD.6] D4 - Dataset User Manual (DUM)
[RD.7] D5-1 - Algorithm Theoretical Basis Documents (ATBD) v1
[RD.8] D6-1 - Product Validation Report (VR) v1
[RD.9] D5-2 - Algorithm Theoretical Basis Documents (ATBD) v2
[RD.10] D6-2 - Product Validation Report (VR) v2
[RD.11] D7 - Experimental Dataset (EDS)
[RD.12] D8 - Experimental Dataset User Manual (EDUM)
[RD.13] D9 - Scientific Analysis and Impact Assessment Report (SciA&IAR)
[RD.14] D10 - Scientific Roadmap (SR)

2 Project overview

2.1 Context

The CryoSMOS project is motivated by potential scientific development and applications that may emerge from the on-going ESA “Soil Moisture and Ocean Salinity” (SMOS) Earth Explorer mission in the Cryosphere domain.

The main objectives of the SMOS mission launched in November 2009 were to measure the surface soil moisture over land and the surface salinity of the ocean. The instrument is a 2D interferometer that measures the microwave emission of the Earth’s surface at L-band (1.4 GHz). The radiometric resolution is about 40km on average, with an ascending/descending orbit at 6am/6pm respectively (solar local time) at the Equator. It covers the entire surface of the Earth within 3 days, thus insuring an interesting time sampling for environmental variables such as soil moisture and ocean salinity. Many applications are being derived from SMOS data, such as a drought index, root zone soil moisture, and assimilation in weather models (ECMWF).

To further exploit and maximise the scientific return of the SMOS mission, a study of the cryosphere has been clearly identified since the beginning of the mission as a second objective. The cryosphere includes the Earth's surface where water is in solid form, i.e. sea ice, lake ice, river ice, snow cover, glaciers, ice sheets, ice shelves, frozen ground and permafrost. This is an essential element of the global climate system, and requires a detailed understanding and monitoring. SMOS mission offers a new point of view for exploring the cryosphere, thanks to a six-year time series performed at a low microwave frequency that has never been used before by a satellite. As observations at microwave frequencies, SMOS gives a very complete time series irrespective of the clouds conditions and without the restriction of daylight (polar nights). However, SMOS differs from higher frequencies by a greater penetration depth in snow (estimated as a few hundred meters at 1 GHz and as a few centimetres at 100 GHz) and a low sensitivity to snow grain size.

Numerous studies have clearly showed the SMOS contribution in obtaining information about sea ice (Kaleschke et al. 2012, 2106, Tian-Kunze et al., 2014, Maaß et al., 2013), frozen soil (Schwank et al., 2004, 2014 and Rautiainen et al., 2012, 2014), etc. However, studies focused on Antarctica are scarce, and require further investigations.

Antarctica is a key element of global climatic system. Its low temperatures (down to -90°C in winter), composition and extension have a vast impact on atmospheric and oceanic circulations, as well as on the Earth’s energy balance. In recent years, considerable changes have been observed across this continent. On the one hand, studies conducted on infrared satellite measurements (which are irregular due to their cloud sensitivity) and on very sparse in-situ data, show that ice sheet surface temperatures are rapidly rising in West Antarctica and in Peninsula, while they seems to be stable in East Antarctica (e.g. Steig et al., 2009). On the other hand, the warming observed in Antarctica has

dramatic consequences on the coastal region. In particular, at present ice shelves (i.e. the floating extension of outlet glaciers) are breaking up while they previously lay undisturbed for at least 10,000 years (Cook and Vaughan, 2010). Several authors have shown that these collapses impact on the glacier dynamics, and thus contribute in rises to sea level (Scambos et al., 2004; Rignot et al., 2011). Therefore, the study of the Antarctic climate requires reliable information on the snow temperatures and firn properties of ice sheet and ice shelves. In addition to the requisites of clearer investigations on the effects of climate changes on the Antarctic continent, there is also a need for better understanding of the geophysical processes taking place there. Indeed, Antarctica dynamics are unique (due to its location, morphology, composition and environmental condition), and are completely different to ones that take place elsewhere.

Because of the sparse coverage of the in situ measurements in Antarctica (Turner et al., 2006) due to the limited possibility of operating in such a harsh environment, remote sensing data are of paramount importance for climate study in this continent. The observations of space-borne sensors are a unique means for providing a detailed picture of the spatial and temporal variations in essential climate variables. Up to now, investigations have been carried out by using optical and microwave satellites. However, due to the frequency bands of the satellite sensors, only the surface of the continent has been extensively investigated. In fact, for a long time (until the launch of ESA SMOS mission) the lowest satellite frequency available was the C-band, which can penetrate the snow for about 50 m. Within this context, SMOS observations have several advantages. Due to the low microwave frequency used (1.4 GHz, i.e. 21 cm wavelength), these observations are sensitive to a higher portion (on the order of 500m or more (Macelloni et al., 2016)) of the ice cap caused by the low snow and ice absorption at L-band. Given the fact that the signal penetration is considerable, the possibility of obtaining information on snow structure on several hundred meters in depth becomes feasible and opens up new research scenarios. Also, since the wavelength is much greater than the dimensions of the snow crystals, the scattering is almost negligible and the emissivity is close to unity when the surface reflection vanishes (i.e. at vertical polarization near the Brewster angle ~50-60deg), suggesting that the brightness temperature is close to the snow temperature.

Therefore, the CryoSMOS project aims to explore the novel capabilities of SMOS to provide innovative observations, new products, and potential future applications within the context of the cryosphere, with special attention to the Antarctic ice sheet, including its floating ice shelves.

2.2 Objectives

In this context, as first objective CryoSMOS focuses on explaining and better understanding of L-band SMOS Brightness Temperature (T_B) observations over the whole Antarctic continent. Starting from this the project aimed to derive experimental scientific products from SMOS data. The analyses explore the influence of snow/ice properties and processes on the T_B and are based on in situ measurements, satellite observations and/or model data as well as on electromagnetic modelling. For an optimal

investigation, it is essential to highlight that various kinds of processes characterise the Antarctic continent. Thus, it is possible to identify several main regions (Figure 2-1): the inner part where the ice-sheet is always dry, the temperature is very low, and the precipitations are scarce; the coast part, where the snow may be wet, the temperature is higher, and precipitations are more intense and frequent; and the ice-shelf region surrounding the continent.

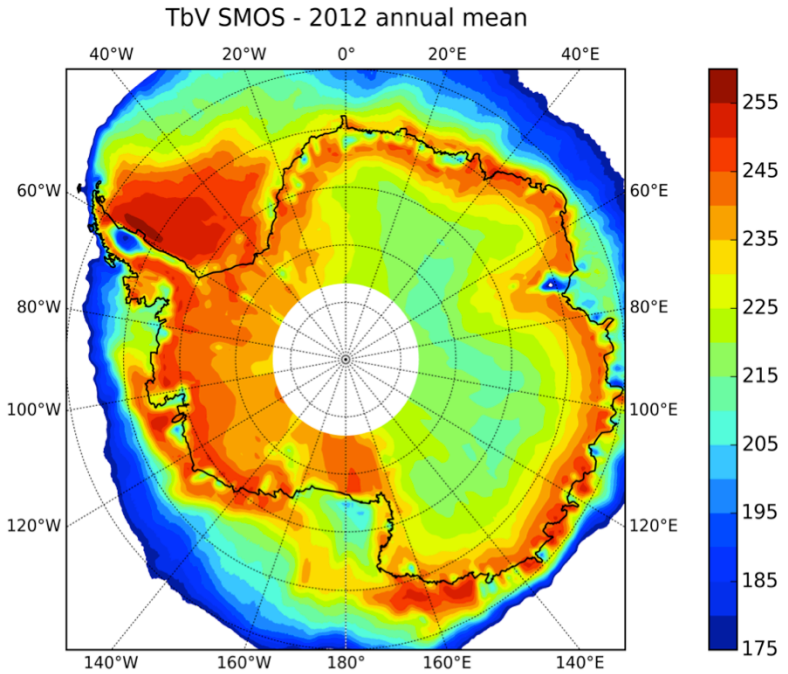

Figure 2-1: Annual SMOS T_B (K) at V-polarization for 55° of incidence angle in Antarctica.

From this consideration, four Case Studies have been defined to investigate SMOS TB in order to take into account the different geophysical processes. These Case Studies focus on:

1. ***the internal temperature of the ice-sheet:***
   The actual temperature profile represents a major unknown in the internal part of the ice sheet. As reported in several papers and books, the dynamics which lead to a given ice temperature distribution are fairly clear and are well-described by thermodynamics laws. However, a determination of the actual temperature profile by using only theoretical approaches is very difficult, since the internal properties of the ice sheet are not completely known (or they are estimated without sufficient accuracy). In this context, brightness temperature measurements at L-band are very valuable for estimating the temperature profile, since they can probe an appreciable part of the ice cap thickness (around 20%-30% in the plateau region), thus providing very useful information.

2. ***the bedrock topography in the inner part of continent:***
   The comparisons of SMOS brightness temperatures over a 350 x 350 km area of ice-sheet covered during the DOMECair campaign (Skou et al., 2015) with the corresponding BEDMAP2 topography

of the bedrock shows interesting correlation. Thus, the question soon came up: can SMOS imagery, which covers all of Antarctica, support our present knowledge about bedrock topography, which is not well known all over Antarctica? The work carried out so far, and reported in Section 5, brings the analysis of the correlation between topography and TB one step further, and consolidates the fact that the choice of this case was correct and promising.

3. ***the ice-shelves:***
   Three important properties of ice-shelves are the thickness, the temperatures, and the state of a potential layer of marine ice. They influence the flow characteristics, and can ultimately determine whether an ice shelve will collapse or not. In order to determine those properties, TB measurements at L-band can benefit from the fact that the ice shelf thickness is less than the L-band penetration depth. The ice temperature of the whole column influences the measured brightness temperature: parts of the signal from below the meteorological ice will penetrate it which might make it possible to estimate its thickness. By analyzing this signal, it could possibly become feasible to estimate its origin (marine ice or water). Marine ice consists of platelet ice crystals that have been produced from ocean water and attached to the meteorological ice, thus partly constructing a consolidated ice layer beneath it. It therefore has very distinct electromagnetic properties, somewhere between fresh meteorological ice and the much saltier sea ice. Since marine ice is softer (because it is warmer), it can prevent the opening of crevasses, and in additions fill up existing ones. By doing this, it is altering the roughness that makes it difficult to predict its exact influence on the brightness temperature.

4. ***the snow surface state on the ice-sheet on one hand and in the coast area on other hand:***
   The state of the surface, i.e. its topographical features and the physical properties of snow in proximity to the surface (grain size, wetness, density), is important to an understanding and prediction the surface energy and mass budgets, which are two key nivo-meterological variables of interest for the study of climate and of the potential contribution to sea level rising. Variations in near surface snow dielectric properties affect radiometric observations, thus providing the possibility of retrieving information about the surface state. Despite the great penetration depth of L-band radiation, snow property changes near the surface (up to one wavelength deep) can impact on SMOS observations. Within this context, an analysis of SMOS observations may provide information about the state of the surface, such as melt events, crust ice, variations in roughness, density, etc.

In the following, Section 3 synthetizes the key findings of each Case Studies as well as the associated experimental final product.

3 Key results

3.1 Case study n.1: Quantifying internal ice-sheet temperature

The internal temperature is a key parameter for the ice sheet dynamics. Indeed all the ice processes, the ease of the ice internal deformations and the rate at which the ice flows across the base, are related to the temperature profile and in turn influence it. At present, the only information about ice sheet internal temperature comes from the small number of boreholes in which temperature profiles have been directly measured and from climate modeling. However, the drilling of boreholes is a very expensive activity (especially due to the ice thickness and the harsh environment) and the current climate or glaciological models are unable to determine the temperature profile at continental scale.

A thoroughly description of the physic of the ice temperature profile can be found in Van der Veen (2013) and in Cuffey and Paterso (2010). The ice sheet temperature distribution is controlled by several factors, the main ones being the climate (which determine the surface temperature), the geothermal heat and frictional heating from basal slip (which can warm and in case melt the base), the ice deformation and meltwater refreezing (which warm the interior) and the mean annual accumulation rate. Also, heat is transferred within the ice layers by their movement in the three directions: a layer can “move” vertically in the glacier due to the accumulation or ablation of the snow on surface, but also can be displaced laterally (advection). Thus the temperature profiles in the ice sheet can be very different from one point to the other.

The simplest case for describing ice temperature profile is the absence of the advection (or its negligible presence) which is a typical condition of the ice divides and domes (e.g. Dome C) and the snow accumulation is low and constant. In this case (also referred as “steady-state temperature profile”), temperature profile is well represented by the model suggested by Robin (1955) and is a function of surface temperature (T_s), ice thickness (H), geothermal heat flux (G), mean accumulation rate (M), ice diffusivity (k_d) and conductivity (k_c):

$$T(z) = T_s - \frac{G\sqrt{\pi}}{2k_c\sqrt{\frac{M}{2k_dH}}}\left(\operatorname{erf}\left(z\sqrt{\frac{M}{2k_dH}}\right) - \operatorname{erf}\left(H\sqrt{\frac{M}{2k_dH}}\right)\right) \quad \text{Eq 3.1}$$

The principal assumptions are that the basal temperature is below the melting point, horizontal heat diffusion is smaller than the vertical one, horizontal velocity of the ice is very small.

3.1.1 Theoretical understanding

Recent studies demonstrate that it is possible to simulate SMOS T_B in Antarctica by using microwave emission models (Leduc-Leballeur et al., 2015; Brogioni et al., 2015; Tan et al., 2015). Nevertheless, the

analyses are focus on Dome C where in situ measurements are available and any theoretical understanding of SMOS T_B spatial variations observed in the inner part of the Antarctica has not been provided before the CryoSMOS project.

The recent paper of Macelloni et al (2016) published by authors of the CryoSMOS team during the project, demonstrated that the T_B spatial variability observed in the inner part of the Antarctica can be mainly attributed to the ice sheet temperature profile variability. In this paper, T_B was simulated by using two microwave emission models (WALOMIS (Wave Approach for LOw-frequency MIcrowave emission in Snow) and DMRT-ML (Dense Medium Radiative Transfer Theory Multi Layer)) using as inputs in particular, the temperature profile provided by the Robin model (Eq 3.1), which in turn depends on the geothermal heat flux, ice thickness, accumulation rate, and surface temperature. These geophysics parameters were found in literature: the geothermal heat flux is available from Shapiro and Ritzwoller (2004) and Fox-Maule et al. (2005), the ice thickness from the BEDMAP2 (Fretwell, 2013), the annual snow accumulation from a climate model coupled with a downscaling algorithm so as to enhance the spatial resolution and to validate accumulations in the in-situ measurements (Agosta et al., 2014), and surface temperature from the Crocus snow model (Vionnet et al., 2012), using forcings from ERA Interim reanalysis (Dee et al., 2011). The temperature profiles computed from these parameters were in good agreement with in situ measured temperature profiles at Dome C and Vostok (RMSE = 0.62K). The density profile, used as model's input to compute the dielectric constant along depth, was derived from previous results (Leduc-Leballeur et al., 2015). The T_B simulation was conducted at V polarization and at the Brewster angle (i.e around 55°) in order to minimize the effect of layering on the microwave emission. Indeed, while it is well known that density increases with depth, ground measurements collected in bore holes demonstrated that each layer exhibits a certain variability with respect to an average value which depends on different conditions and processes occurred during the layer's formation (i.e snow accumulation, wind speed, surface temperature, etc.). This variability is unknown outside of the few places where measurements were collected but it strongly influences the dielectric constant of the ice sheet and then its emission except at V polarization and at the Brewster's angle when the surface and internal reflections vanish.

It is also worth mentioning that, whereas the analysis was focused to the description of the V polarization near the Brewster's angle, the similar T_B features were visible at different incidence angles and at H polarization, although with different T_B values. This implicitly confirms that the temperature profile, together with the main glaciological parameters on which it depends, plays a major role in understanding SMOS signature signatures.

A key point for microwave emission models simulation is the selection of the ice permittivity model. The real part of ice permittivity is usually well known: it is constant over the microwave range, depends mostly on the snow density, and has a weak dependence on temperature. In contrast, the imaginary part is more uncertain because of the difficulty of measuring it due to its very low magnitude. It controls the penetration depth, and the sensitivity to the temperature profile in view of that extinction is largely dominated by absorption. Two different empirical formulas deduced from

measurements were tested: Mätzler (2006) and Tiuri et al. (1984). A comparison of the imaginary part of ice permittivity, as computed by the two models at the SMOS frequency (i.e. 1.413 GHz) demonstrated that the Mätzler formulation (referred to as the MA here as follows) has a lower value and a more reduced sensitivity to ice temperature than the Tiuri formulation (referred to as the TI here as follows). Indeed, when the temperature increases from 220K to 270K, the imaginary part of the ice permittivity increases from 0.06 10^{-3} to 0.5 10^{-3} with the MA formulation and from 0.3 10^{-3} to 1.65 10^{-3} with the TI formulation.

Using the above models, the SMOS T_B was simulated for both the TI and the MA formulations of the ice permittivity over three transects in the inner part on the East Antarctic Plateau. For each transect, simulations were performed every 10 km, using the temperature profile as input and assuming the density profile to be constant along the transects. The results for the three transects clearly demonstrate that by using TI it is possible to correctly simulate the absolute T_B value at Dome C, where the model was previously tested (Leduc-Leballeur et al., 2015, Brogioni et al., 2015). Moreover by using TI, the model overestimated the SMOS T_B by about 2.5 K on average over the three transects. When the MA formulation was used, the simulated T_B was overestimated by about 8.5 K in all the transects including Dome C. However, it is worth noting that the T_B followed the SMOS fluctuations satisfactorily in all three transect. The discrepancy between model and data was independent of the microwave emission model used. As an example, Figure 3-1 shows the comparison between T_B measured by SMOS and simulated by the microwave emission models by using the two permittivity models. The figure shows the $\Delta T_B = T_B$ along the transect - T_B measured at Dome C.

After an in depth discussion of all the elements were considered in the model simulation, we concluded that the main source of incertitude is the permittivity model. The MA formulation yields the largest warm bias (8.5K). However, it seems to be more appropriate in reproducing the T_B variations, whereas the TI formulation provides a good agreement at Dome C and yields a moderate bias (2K) along the transects. In any case, the simulated spatial variations are weaker than the observed ones.

By way of a summary, the above discussion points out that, by using an appropriate glaciological and microwave emission model is possible to theoretically understand the SMOS T_B variability. The remaining differences between simulated and observed SMOS T_B (mainly a bias) can be attributed to the formulation of the ice sheet permittivity. On the other hand, these results are not surprising because the ice permittivity models were developed for very high ice temperature (i.e. 240K to 270K, instead of 220K) and the values of the imaginary part of the ice are very low (around 10^{-3}-10^{-4}). The latter, in turn, has an impact on the accuracy of the measurements.

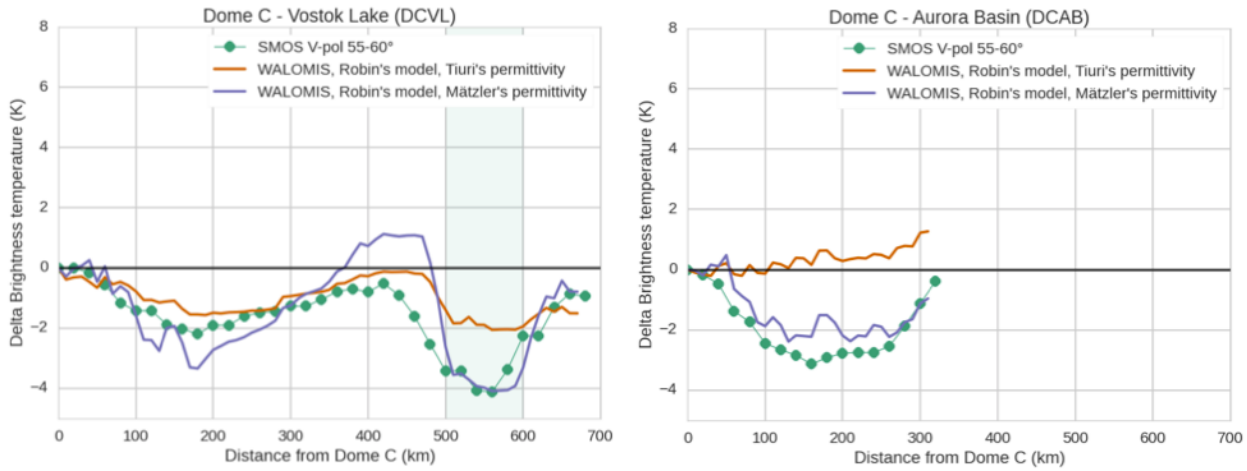

Figure 3-1: ΔT_B (i.e. T_B along the transect - T_B measured at Dome C) at V polarization for SMOS (green dotted line), and WALOMIS simulated T_B (orange = Tiuri's permittivity; purple = Mätzler's permittivity) as a function of the distance from Dome C along two transects. The shaded blue area indicates Lake Vostok (from Macelloni et al. 2016).

3.1.2 Retrieval approach

The ice sheet temperature profile retrieval is performed at SMOS pixel scale and it is based on the minimization of a cost function whose kernel is the mean square error between the SMOS measurements and the simulated T_B by the WALOMIS model above described. This latter use as inputs the temperature profile described by the Robin's model, the MA permittivity model which consider a bias correction to take into account on the above mentioned difference and a density profile was obtained from measurements at Dome C. A regularization function, which accounts for the variability of the physical parameters to be retrieved, is included.

For each SMOS pixel, iterations are performed over two free variables of the Robin model (the geothermal heat flux and the annual snow accumulation), which can vary around the first guess obtained from the a-priori information (i.e. from literature). Two other model parameters, namely the ice thickness (H) and the surface temperature (T_s), which have a low incertitude, have been taken from literature. The cost function is computed for every allowed pair of G and M, then the minimum is determined and the associated optimal pair (G_{opt}, M_{opt}), i.e. the pair that makes the simulated T_B to minimize the cost function, selected for the ice sheet profile estimation. Finally, the Robin model is run again to calculate the retrieved temperature profile using as inputs T_s, H, G_{opt} and M_{opt}.

It is worth recalling that the Robin model, used to estimate the ice temperature, is valid for regions characterized by a negligible horizontal advection. These regions are essentially the ones, which experienced a very slow horizontal movement and are mainly located in the internal part of the East Antarctic Plateau.

Data Pre-Processing

The retrieval is composed by several steps the first one consists in the pre-processing of inputs data, which are first of all re-projected and co-registered on the EASE2 grid (Figure 3-2).

The first step of the pre-processing is the elimination from the five input maps (SMOS T_B at V polarization close to the Brewster angle, T_s, H, G and M) of all of those pixels that lies outside the Robin model validity mask. Also, since the sensitivity of T_B to the ice thickness is on the order of 1K per 300-500 m of ice thickness, all of the areas whose ice thickness is lower than 1000 m were disregarded since the error on the SMOS measurements is on the same order of the ice sheet emitted T_B.
Then the SMOS L3 data are temporally averaged in order to have a T_B map representative of the emission over a long time period. It is expected that the T_B at L-band cannot have appreciable temporal variations, thus all of those pixel with a temporal standard deviation greater than 1 K were disregarded.
After having spatially filtered the input datasets and also temporally averaged the SMOS measurements, the pre-processing is concluded and all of the data are ready to be used in the retrieval algorithm.

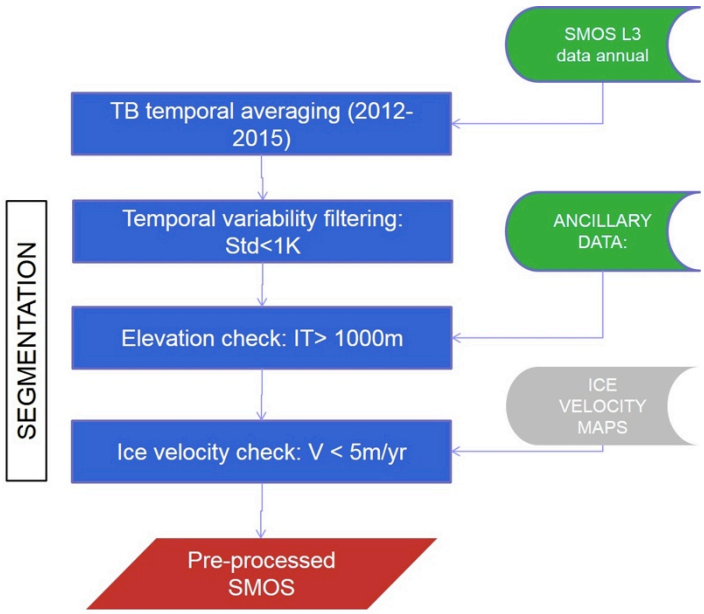

Figure 3-2: Pre-processing of SMOS L3 data.

In Figure 3-3 are shown the regions over which the ice sheet temperature profile retrieval will be performed. The threshold applied were: standard deviation of T_B at V polarization lower than 1 K, ice thickness higher than 1000 m, surface balance velocity lower than 5m/yr (green) and between 5 and 10 m/yr (blue). Robin model strictly applied in green regions, however the retrieval is performed also in blue area with a lower confidence. Every pixel is marked with a specific confidence flag to reflect these two conditions.

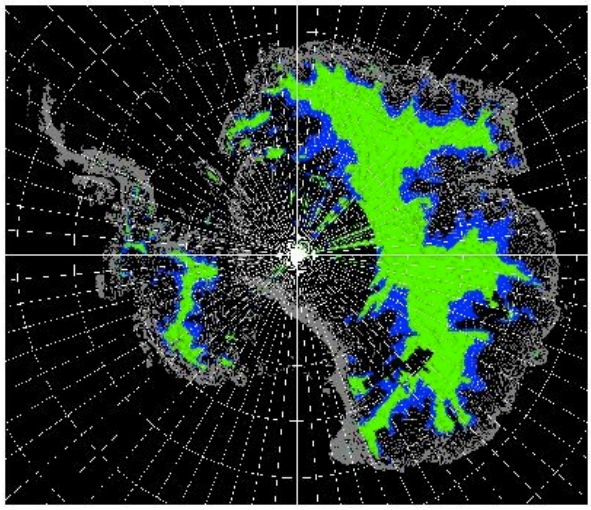

Figure 3-3: Mask of applicability of the ice sheet temperature profile retrieval. The green and blue areas indicate surface balance mass velocity lower than 5m/yr and between 5 and 10 m/yr respectively, standard deviation of T_BV lower than 1K, ice thickness higher than 1000 m.

The Cost Function (CF)

As mentioned the retrieval is based on the minimization of a cost function for two parameters (G, M). For each combination of (G, M) the CF is described as follows:

$$CF(G,M) = \frac{1}{N_\theta}\frac{1}{\sigma_{TB}^2}\sum_{\theta=\theta_1}^{\theta_n}\|T_{b\,SMOS}(\theta) - T_{b\,WALOMIS}(\theta,G,M)\|^2 + \frac{1}{\sigma_G^2}\|G_{anc}-G\|^2 + \frac{1}{\sigma_M^2}\|M_{anc}-M\|^2 \quad \text{Eq 3.2}$$

where:

- $T_{b\,SMOS}(\theta), T_{b\,WALOMIS}$ are the measured and simulated T_B for different incidence angles (θ),
- G_{anc}, M_{anc} are the geothermal heat flux and accumulation a-priori values,
- σ_{TB}, σ_G, σ_M are the standard deviation of SMOS T_B, geothermal heat flux and snow accumulation, respectively. σ_{TB} is calculated with T_B annual average, the other values are available from literature,
- N_θ is the number of incidence angles considered in the retrieval.

In order to optimize the CF configuration several tests were carried out. The parameters tested were: the number of angles close to Brewster one to be considered; the number of pixel which be considered; the a-priori search range for the basal heat flux G and the accumulation M; if to consider or not the regularization term. For each configuration, the retrieval of the ice sheet temperature profile was performed over a selected transect on the East Antarctic Plateau where ground data are available (i.e the one from Dome C (DC) and Vostok (VL), Figure 3-1, left). In this transect, we considered the error of the estimates of G and M at DC and VL test sites, the RMSE and the mean bias between SMOS and WALOMIS simulations over the entire transect. The analysis points out that the

best configuration is to consider three incidence angles, the regularization function and to exclude near pixels. For each pixel, the G and M ranges are the-priori value ±50% and ±20%, respectively. By using this configuration, the retrieval is performed for each pixel of Antarctica where the retrieval is feasible (i.e. see Figure 3-3). Figure 3-4 shows the fitting of the SMOS measurements and the values of the cost function (and its components) as a function of the distance from Dome C. It can be observed that the RMSE between SMOS and simulated T_B is 0.46 K.

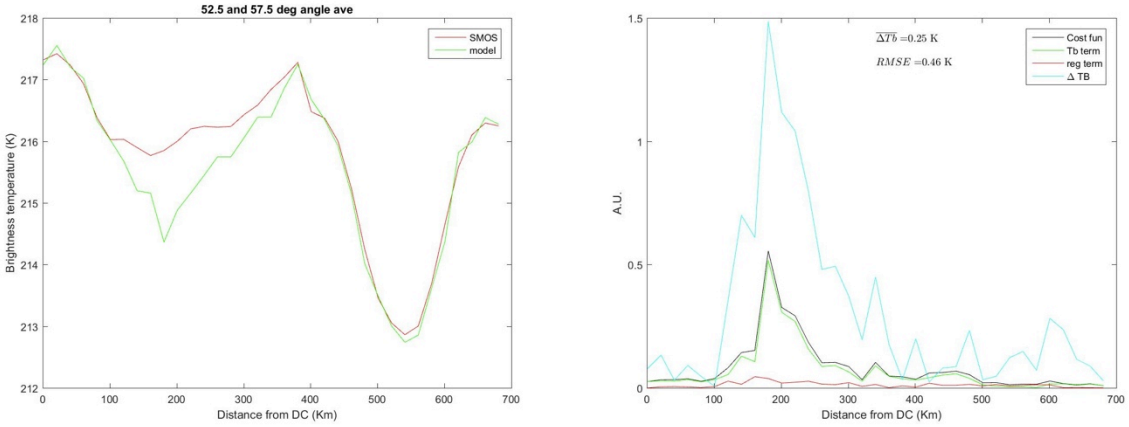

Figure 3-4: (left) Measured (red) and fitted (green) T_BV, and (right) the Cost Function (black) and its components Tb_MSE (green) and regularization term (red), along the transect from Dome C to Vostok Lake. The difference between measured and fitted T_BV (light blue) is also superimposed to the Cost Function.

3.1.3 Experimental final product

The final product is the temperature profile of Antarctica at different depths. Areas where Robin model is not valid are masked out and a quality flag with the confidence of the estimation also provided (Table 3-1). The quality has been classified on the basis of the score of the minimum Cost Function. Low quality (quality=2) is assigned to areas where the CF value is higher than 2, while the best quality (quality=0) is for CF lower than 1.5. Moreover, the retrieval of the ice sheet temperature performed in the regions characterized by a surface balance velocity between 5 m/yr and 10 m/y is flagged as low quality.

Table 3-1: Values associated to the different quality of temperature profile retrieval

FLAG VALUE	QUALITY	CONDITIONS
0	Good	CF<=1.5
1	Medium	1.5<CF<=2 or (G_{opt} = a-priori ± 50%) or (M_{opt} = a-priori ± 20%)
2	Low	(CF>2) or (5 m/yr < surf velocity < 10 m/yr)
NaN	Retrieval Not Feasible	N/A

A first check to assess the retrieval goodness over Antarctica is the comparison between simulated T_B and SMOS (Figure 3-5). The error is less than 5K over the entire retrieval mask, but can be differentiate between two distinct areas having different surface balance velocities (Figure 3-3). In the first area (velocity < 5m/year), Robin's model is strictly verified and the simulated T_B can reproduce very well SMOS showing an error of less than 1K. The second area is basically the boundary of the first one corresponding to a relaxation of Robin's conditions (velocity is between 5m/yr and 10m/yr) and where the retrieval product is admitted with lower quality (quality flag=2). In this area the error is always between 1K and 5K, which is higher than in the first area.

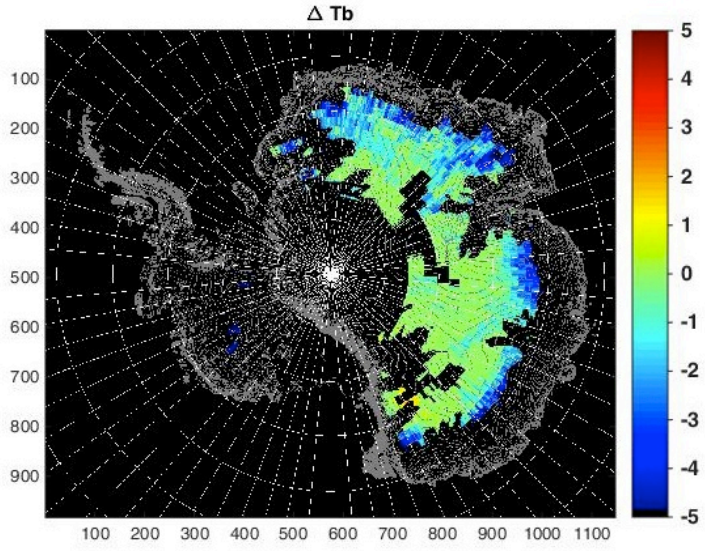

Figure 3-5: Difference between simulated T_B and SMOS over Antarctica. Values are obtained averaging the T_B over the incidence angles used for the retrieval.

Figure 3-6 shows the retrieved ice temperature maps obtained at 50m, 250m, 500m, 1000m, 1500m and 2000m depths. Temperature at first 50m below the surface is spatially homogeneous and strongly influenced by surface temperature. Temperature increases with depth according to Robin's equation and reaches the warmest close to the bedrock. Spatial variability of the retrieved temperature considerably changes from 1000m depth and it is more affected by bedrock topography and geothermal heat flux distribution.

Error Analysis

An analysis of possible error sources has been also conducted in order to define incertitude of the delivered products. A first kind of error is the one produced by the uncertainty of ancillary data considered in the retrieval: i.e. the mean surface temperature (T_s) and the ice thickness (H). Another important parameter is the offset value, which has been calculated in order to correct the T_B simulations (RD.9, RD.10). This value is applied to the microwave emission model output, which overestimates T_B of several kelvins compared to SMOS. The optimum value of the offset has been firstly computed for Dome C and Vostok area, then validated along a 700 km transect. However, since

it was not evaluated everywhere, the uncertainty on this parameter must be included in the error analysis. Errors on the a-priori information are not considered since these are the parameters, which are used for the minimization of the cost function. Indeed, the range of variability of these parameters, which is used in the minimization, is considered to be enough large to compensate a potential error in the selection of their initial values.

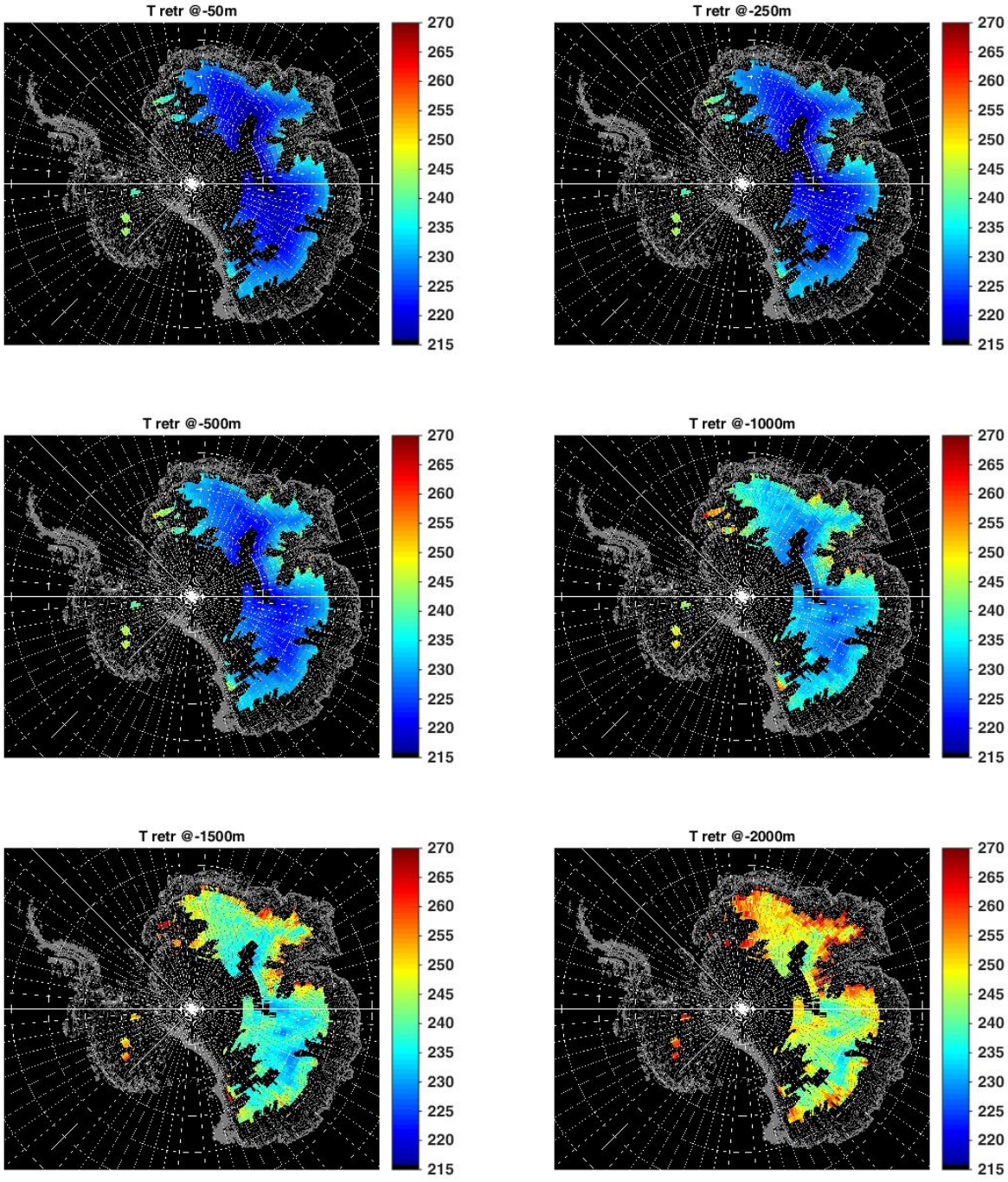

Figure 3-6: Retrieved ice temperature maps at 50m, 250m, 500m 1000m 1500m and 2000m depth.

Errors on microwave emission model are not considered because previous studies demonstrated that, if reliable inputs are available, the model is able to reproduce SMOS T_B (Leduc-Leballeur et al., 2015, Macelloni et al., 2016). Regarding the Robin model used for the temperature profile, it has been widely used in the glaciological community and its ability in reproducing the temperature profiles in Antarctica is well documented. Results on the retrieved ice sheet temperature profiles confirm that, below 500m depth, effect of uncertainty on T_s and H is quite low and similar, with RMSE lower than 1.78K at 2500m depth, while effect of the offset is much higher with RMSE lower than 4.06K at 2500m depth. Considering the error on offset, it must be considered that, the determination of the offset value is based on the two temperature profiles, which are now available. Further refinement will be possible in the future if new measurements could be available. It is worth noticing that the increasing of the error with depth is not surprising since the L-band T_B is sensitive to the temperature up to 2000m (Macelloni et al., 2016) and the maximum performances of the retrieval are achieved within this depth. In this respect, the use of lower frequencies, as suggested in Jezek et al. (2015) can be able to improve the performances even at lower depth.

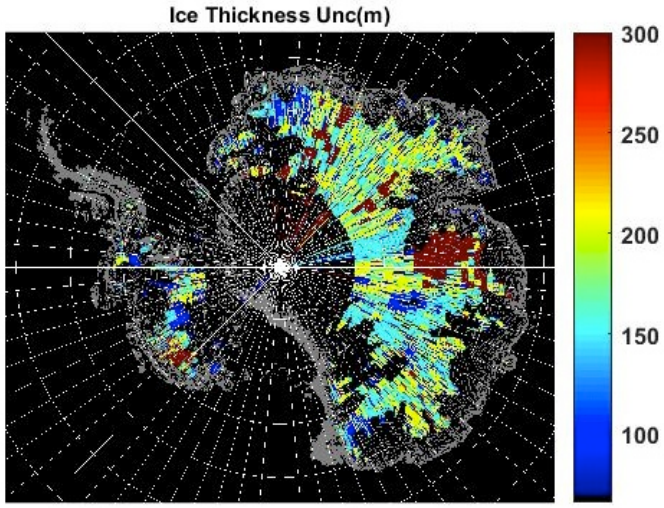

Figure 3-7: Ice thickness uncertainty from Bedmap2 after applying retrieval mask. Dark red corresponds to the 1000m uncertainty.

In order to provide an error estimation for each SMOS pixel where the products will retrieved, only the uncertainty on ice thickness can be considered since it is the only auxiliary parameter with a good error estimation. Indeed, the error on surface temperature is not well quantified all over Antarctica, although some discrepancies of 0.3 K are observed in some regions (Fréville et al., 2014). These differences can be positive as well as negative but, because of the lack of a consistent dataset of ground measurements to validate the T_s model estimations, we have to admit that the error cannot be quantified. On the other hand, previous analysis (D5.1) already provides an overview of the expected impact on the temperature profile on an error on the estimation of this parameter. Error on the ice thickness estimation is provided in Bedamp2 project (Figure 3-7). Starting from this data, an error map

for the temperature profile has been generated for different depths below surface (Figure 3-8). For a given depth, the represented error is the difference between temperature retrieved by considering the nominal depth and the one with the nominal depth plus or minus the H incertitude. Also in this case, if new data will be available the uncertainty maps can be improved.

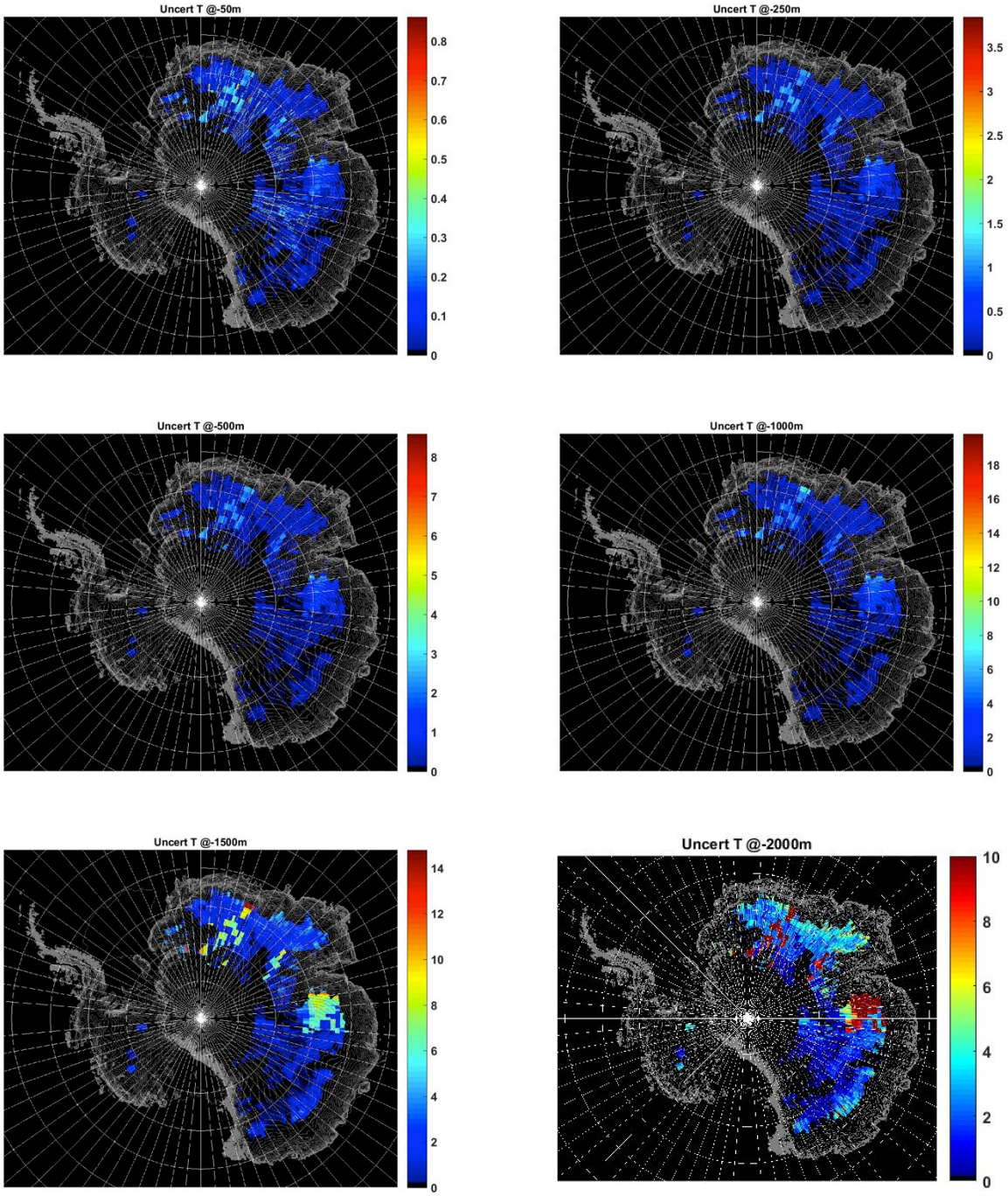

Figure 3-8: The retrieval error due to uncertainty on ice thickness by Bedmap2 at different depths below surface: 50m, 250m, 500m, 1000m, 1500m, 2000m

3.1.4 Products Validation

Because of the lack of snow ice cores it is quite difficult to compare these results with real in situ data and then validate it. Indeed, the only two available deep ice cores, were collected at Concordia and Vostock bases, were used to assess the methodologies. Nevertheless, in order to evaluate the obtained results the temperature values can be compared to those obtained by a glaciological model.

The Glaciological Model

Temperature profiles dataset used here for comparison with retrieval ones come from the study of Van Liefferinge and Pattyn (2013). The authors used a three-dimensional thermodynamical model especially dedicated to model the Antarctic ice-sheet (Pattyn, 2010). They used several global Antarctic datasets to setup the model. Bedrock topography is based on BEDMAP2 (Freetwell et al. 2013). Surface temperatures are provide by van den Broeke (2008), based on a combined regional climate model, and calibrated with observed 10 m ice temperatures. Surface-mass balance is obtained from van de Berg et al. (2006) and van den Broeke et al. (2006). The temperature field in the Antarctic ice sheet was calculated for 15 different sets of boundary conditions: the three data sets of geothermal heat flux (Shapiro and Ritzwoller, 2004; Fox Maule et al., 2005; Purucker, 2013), and each of the data sets corrected for subglacial lakes and existing temperature profiles. The ensemble of 15 experiments is averaged and this dataset is used in the following.

In order to verify the added value of the developed methodology, we first compare the simulated Tb to the SMOS data. Two cases are considered for the temperature profile used as inputs of the WALOMIS model: 1) profiles generated by the glaciological model; 2) profiles obtained by using the Robin model before (i.e. by using the a-priori values) and after the minimization (i.e at the end of the retrieval). Indeed, if the same results were obtained for the 2 cases, it could be concluded that the glaciological model provides reliable results and, consequently, the impact of SMOS measurements on the temperature retrieval is negligible.

Figure 3-9 shows the comparison between SMOS and simulated T_B computed by using the Robin model with a-priori data (left) and the glaciological model (right). It can be noticed that when Robin model is used we obtain, as expected, the same bias, which was assumed for the minimization (see D5 for details) and a RMSE of 1.14K. As explained the bias is motivated by the current limits of the permittivity models. If the glaciological model is used, the data are more scattered (i.e. RMSE is higher: 1.36K) and the bias is lower of about 1K. Results obtained by using the profile obtained from the minimization are presented in Figure 3-10. The agreement between simulated and SMOS T_B largely improved while the bias remained almost the same. In this case, the RMSE is of 0.45K. These results imply that by using the temperature profile provided by the glaciological model we are not able to appropriately represent the SMOS T_B or that the temperature profile is not completely correct. This result is somewhat expected since, it is well known, that the glaciological model is affected by the incertitude of some of its geophysical parameters. As an example, the ice thickness obtained from

Bedmap-2, has an incertitude that ranges from few meters up to 500-1000 m. Moreover, the geothermal heat flux is also affected by large errors, which are mainly due to the lack of data. In Van Liefferinge and Pattyn (2013) the source of error in computing the basal temperature is clearly shown.

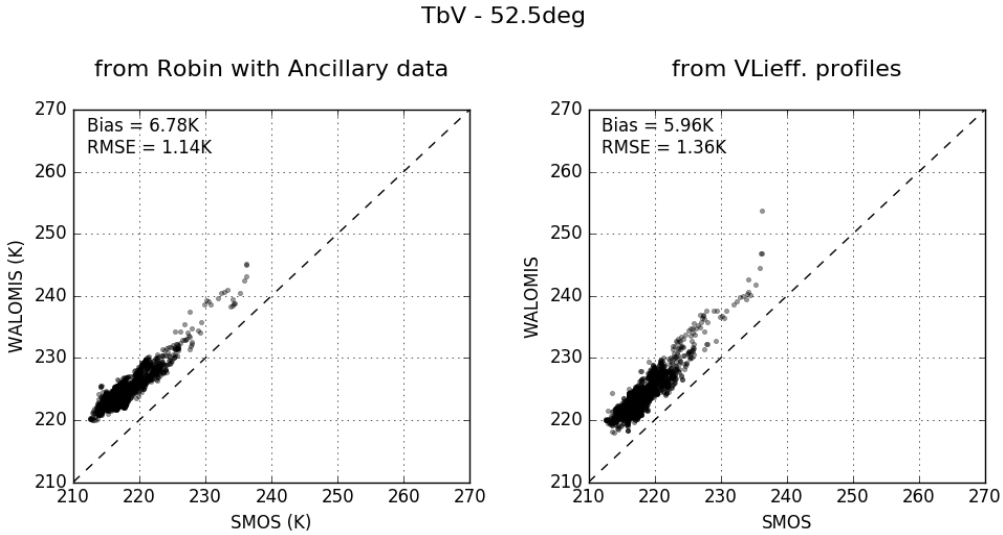

Figure 3-9: Differences between SMOS and the WALOMIS T_B simulated with temperature profile (left) from Robin model and a-priori data, (right) from glaciological model.

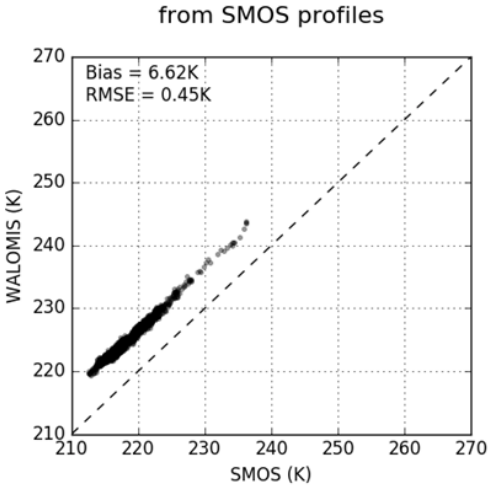

Figure 3-10: Differences between SMOS and the WALOMIS T_B simulated the temperature profiles obtained after the minimization.

The temperature profiles obtained from the two methodologies are then compared for the whole plateau. Figure 3-11 shows the temperature differences (i.e. derived by SMOS and by glaciological model) computed at the surface level and 100 m far from the bedrock. It can be noticed that while on the surface the temperature is very similar it can be significantly different close to the bedrock. In detail pixels at longitude between 100 E and 140 E show in general colder values while the other pixels exhibit higher temperatures. The differences of temperature can ranges from +10 °C to -10 °C.

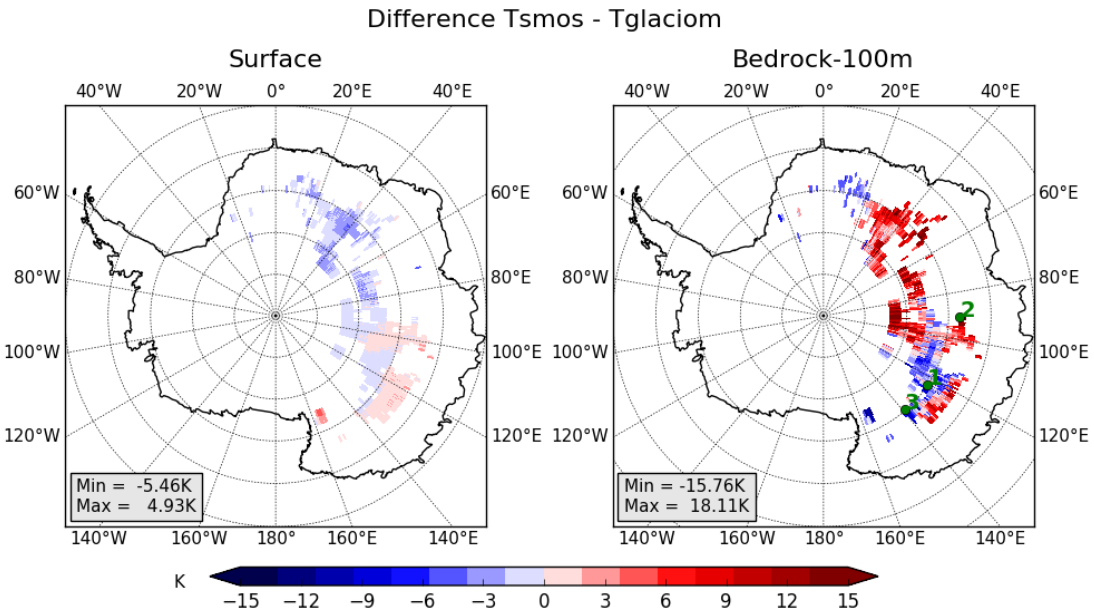

Figure 3-11: Differences between the ice sheet temperature computed from SMOS and derived from glaciological model at the surface (left) and at 100 m far from the bedrock (right).

Detailed analysis is presented in [D.9] but as general summary it can be observed that, in several cases, the temperature profile retrieved by SMOS differs from what is predicted by the glaciological model. Nevertheless it is quite difficult to demonstrate, which results are the most reliable because of the lack of measured temperature profile that can be used for comparison. The difference between temperatures is not systematic, varying points by points and can be either positive or negative. However, it has been observed that main differences are observed close to the bedrock and this is motivated by the following reasons:

- The incertitude of the geothermal heat flux, which is the main responsible of the basal temperature in the glaciological model and which is used as the starting point for the minimization in the SMOS algorithm.
- L-band T_B is mainly sensitive to the microwave emission of the first part of the ice sheet (i.e about 1500 -2000m; Macelloni et al. 2016), and the contribution of the last part has a minor impact on the total emission (i.e. lesser than 10 %, Macelloni et al. (2016), Fig. 7). This implies that an error in the temperature profile in this part has a marginal effect on the simulated T_B. A difference of temperature of 11K or 14K at the bottom implies a difference of about 2K on T_BV at an incidence angle of 52.5°.

This last point suggests that the reliability of SMOS derived products for the second half of the ice sheet thickness must be considered with caution. In particular, where the temperature at the bedrock provided by SMOS largely exceeds the incertitude range predicted in literature for the basal temperature. In any case, the accuracy of temperature provided by glaciological model is also questionable for the above mentioned incertitude on geophysical parameters.

3.1.5 Additional Derived Products

Besides the temperature profiles the retrieval procedure provides two other parameters, which are used in the minimization: the geothermal heat flux and the accumulation. In the following sub-sections the results obtained by the retrieval are compared to the ones found/provided by literature.

Geothermal heat flux

The Geothermal Heat Flux dataset used here was obtained from Fox Maule et al. (2005) (data contained in ALBMAP database available on https://doi.pangaea.de/10.1594/PANGAEA.734145; (Le Brocq et al., 2010). The authors precise that, due to some assumptions, the estimated error for geothermal heat flux map is in the order of 21-27 mW m^{-2}.

The absolute and percentage difference between retrieved and literature geothermal heat flux are shown in Figure 3-12. The figure shows that the difference is between -25 mW m^{-2} and +20 mW m^{-2} corresponding to a variation of ±25% at maximum with respect to the literature values and in agreement with the uncertainty of the product mentioned above. Moreover the map shows that the heat flux is higher in certain regions and lower in other and that the difference is quite independent of latitude, longitude and ice thickness. The results is not surprising since it is well known that, due to the lack of direct measurements, the geothermal heat flux is affected by a large uncertainty. For example, Van Liefferinge and Pattyn (2013) demonstrated that by using a combination of several models (i.e. Fox Maule et al. (2005), Shapiro and Ritzwoller (2004), Purucker (2013)) in the regions of Antarctica considered here, we obtain an average value of 55 mW m^{-3} and a standard deviation of about 30 mW m^{-3} is obtained.

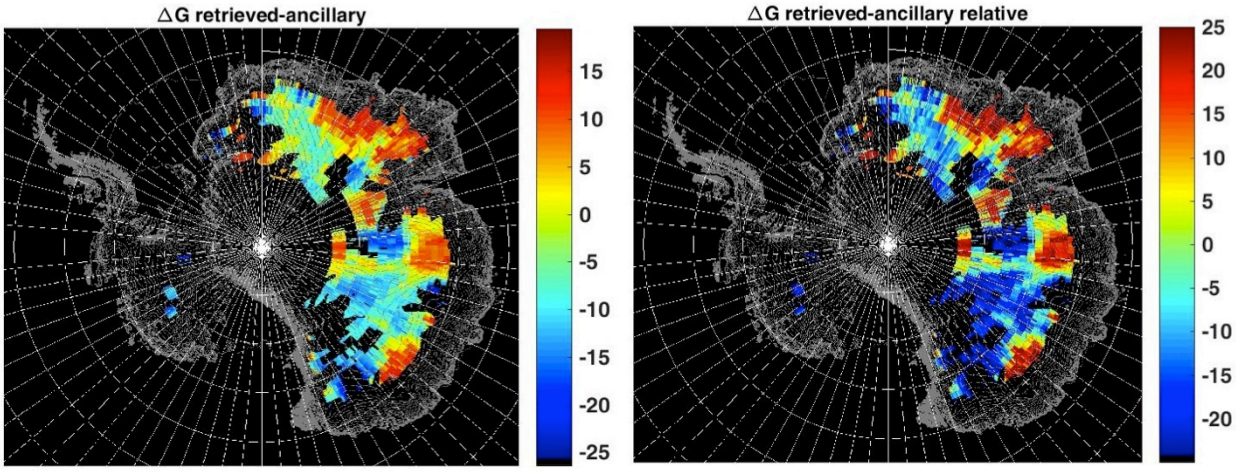

Figure 3-12: Difference between retrieved geothermal heat flux and the one from ALBMAP (left) and in relative percentage (right) for the whole considered pixels.

Snow Accumulation

The snow accumulation dataset used here are provided by LGGE according to Agosta et al. (2013) using the RACMO model (Regional Atmospheric Climate Model). The estimated error is in the order of

0.003 m/yr. The absolute and percentage difference between retrieved and model accumulation is represented in Figure 3-13. In this case the difference between model and SMOS estimated product is very low and, except in the marginal zone of the map, it did not exceed the 10%.

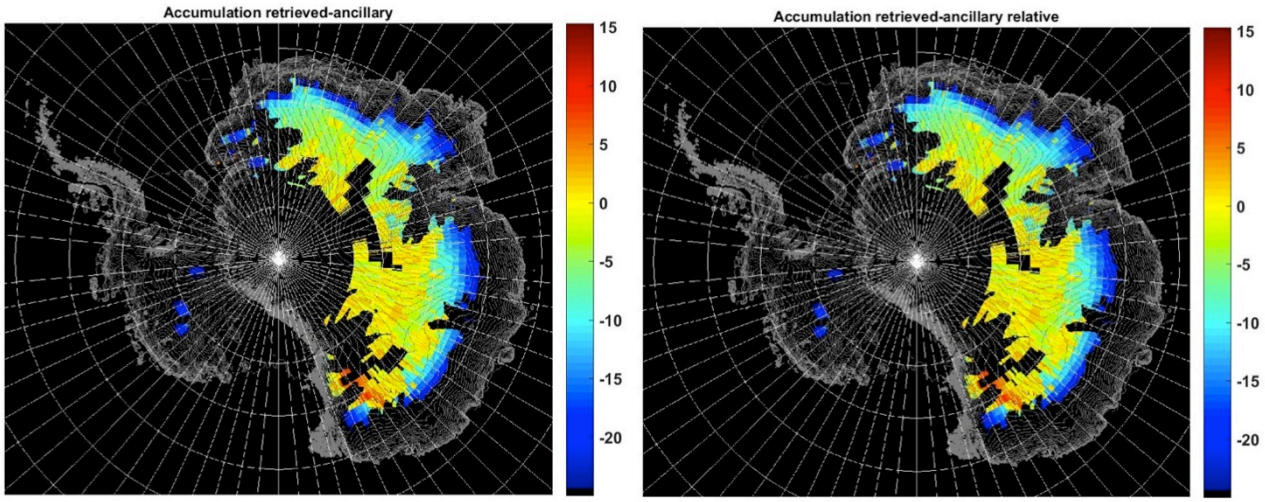

Figure 3-13: Difference between retrieved accumulation and the one from Agosta et al. (2013) in absolute (left) and in relative percentage (right) for the whole considered pixels.

3.2 Case study n.2: Bedrock topography and/or geothermal heat flux

In January 2013, the 1.4 GHz DTU radiometer system was flown over a 350 km by 350 km area near the Italian/French Concordia station close to Dome-C in Antarctica (Skou et al., 2015). Vertically and horizontally polarized brightness temperatures (T_B) at 45° incidence angle and at nadir were acquired. The ice surface is quite flat at a level of some 3000 m above sea level. A grid of 11 flight lines separated by 35 km was flown. The yearly mean temperature in the area is -55°C corresponding to 218 K.

The purpose of the campaign was to check the spatial homogeneity of the T_B in the area. The original assumption was that the penetration depth in the ice at L-band would be such that the prime contribution to the T_B would be the cold and thermally stable ice some hundreds of meters down – that is, no variations both temporally and spatially. This would constitute a well-known and stable target for calibration and inter-comparison of spaceborne L-band radiometer systems.

The measured T_B, however, show unexpected variations like 8-K variation over a 240 km east – west profile through Concordia, and in certain local cases, a slope of about 0.7 K/km. Comparing the measured T_B (Figure 3-14, left) with bedrock topography (Figure 3-14, right) reveals a convincing correlation.

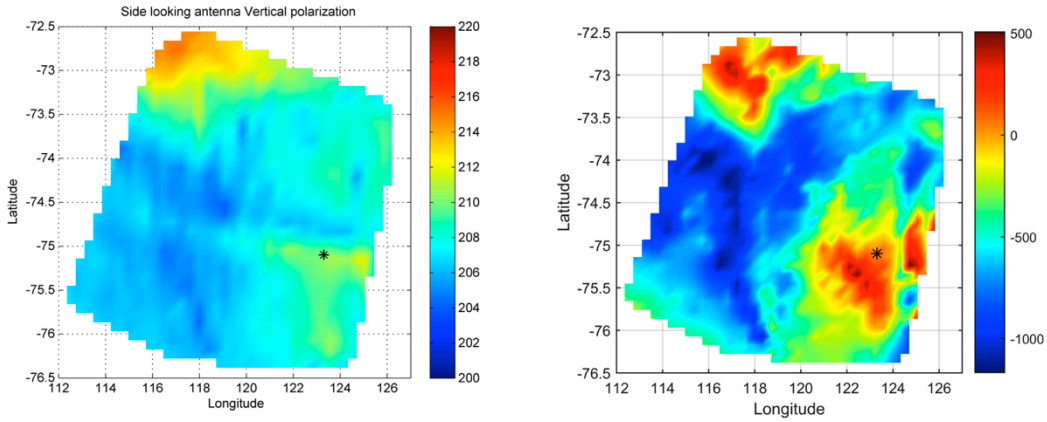

Figure 3-14: T_BV (K) map of the Concordia are (left) and bedrock in m above sea level (right).

Simulations, using realistic temperature profiles and current knowledge about ice loss, show that variations in bedrock topography, hence ice thickness, can indeed modulate the T_B appropriately to explain the observed variations. It is concluded that SMOS T_B maps can indicate ice thickness hence bedrock topography in Antarctica.

It is assumed that the findings over the test area near Concordia can be used over large parts of Antarctica, excluding coastal areas. Figure 3-15 taken from Fretwell et al. (2013) shows the uncertainties in the current estimates of the ice thickness, which propagates almost directly into the uncertainty in bedrock, as the surface is well known. It is evident that our interest should focus on the larger red areas, where uncertainties are around 1000 m! These are not coastal areas, and especially the area near Lake Vostok (centrally located in East Antarctica) will have ice properties not very different from the test area. This is our target area.

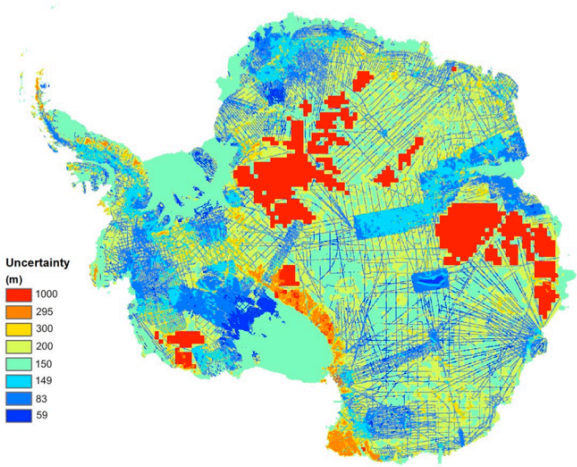

Figure 3-15: Estimated uncertainty in ice thickness (Fretwell et al., 2013).

3.2.1 Theoretical understanding

The bedrock elevation in our test area ranges from some −1000 m to about +500 m compared with sea level, i.e., the ice thickness varies by some 1500 m. So, the question is: can this ice thickness variation, due to bedrock topography, in areas with some 3 km of ice (the surface is around 3000 m) affect the T_B to the observed level?

One possible explanation is that the penetration depth at L-band is substantially greater than originally assumed. The physical temperature in the ice ranges from −55°C near the surface to about 0°C near bedrock due to geothermal heat. Hence, at a certain depth, deep in the ice, the temperature will vary according to the bedrock elevation. Varying ice temperature means varying absorption of microwaves. If the radiometer looks to this depth in the ice, these variations will result in T_B variations.

Numerical radiative transfer simulations using current values for the absorption coefficient of dry, Antarctic ice and realistic temperature profiles have been carried out. The absorption coefficient increases from 0.09/100 m at −55°C to some 0.8/100 m at 0°C (Figure 3-16).

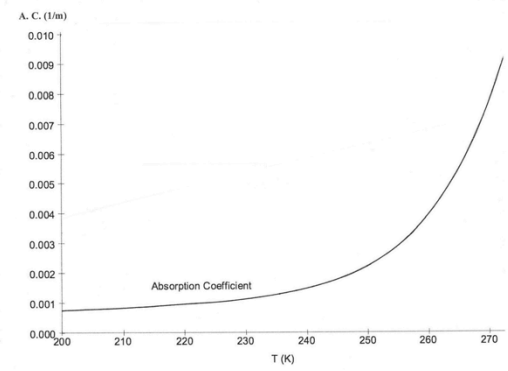

Figure 3-16: Absorption coefficient per meter in ice.

As already discussed, the temperature in the ice ranges (apart from the top 10–20 m or so where seasonal variations are observed) from 218 K at shallow depth to about 270 K at the bedrock. Oftentimes an exponential profile is considered, but actually, the shape is dependent on a range of parameters including yearly accumulation. An almost linear curve is typical for a very low accumulation of 1 cm/year, while more exponential-looking curves are found for up to 5 cm/year. The accumulation at Concordia is at the low end of this range. Hence, it has been decided to carry out these simple simulations three times using two exponential temperature profiles and a linear profile.

Actually, we have available a measured temperature profile from Vostok, also in the Dome-C area. This profile is quite representative for Concordia (both stations have quite similar conditions and little accumulation). Figure 3-17 shows the Vostok profile and the three profiles used in the simulations. It is noted that the Vostok profile is between the red exponential and the linear profile (right panel) used in the simulations.

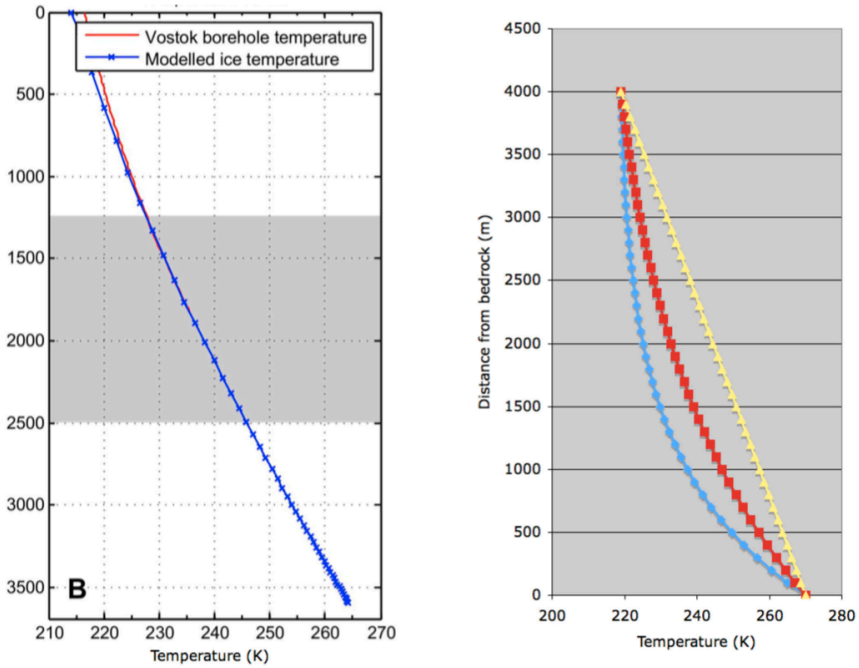

Figure 3-17: Measured temperature profile (K) at Vostok (left) and the 3 representative profiles (right).

Two different ice thicknesses will be dealt with: 2500 and 4000 m to illustrate the conditions near Concordia.

Having the absorption coefficient from Figure 3-16 and the temperature from Figure 3-17, the T_B is found from successive application of the following formula for a single layer in layered media:

$$TB_{out} = TB_{in} \cdot (1 - ac) + T \cdot ac$$

where TB_{in} is the T_B entering the layer, ac is the absorption coefficient, T is the physical temperature, and TB_{out} is the outgoing T_B. Layers with a thickness of 100 m are used, and layer no. 1 is at the bedrock. TB_{in} for this first layer is assumed to be 273 K due to the wet/lossy conditions here.

The result is that the T_B at the ice surface is modulated by some 4 K for the ice thickness (hence bottom topography) varying by 1500 m - and there is no significant difference between the exponential and the linear temperature profiles. The simulated 4 K variation compares well with the measured T_B variations in the southern part of the test area, where the physical -10 m temperature is known to be quite uniform.

In conclusion: using a simple exponential temperature profile for each data point, forced to be 270 K near bedrock and the -10 m temperature near the ice surface, simulations show that the T_B is indeed modified in an understandable way by ice thickness. Hence, ice thickness – and thereby bedrock topography – can be found from L-band T_B measurements.

3.2.2 Retrieval approach

Correction for the -10 m temperature

In our test area around Concordia the -10 m temperature varies by some 9°C. This must be corrected for, but since the ice is in fact not a perfect blackbody the temperature must be multiplied by a factor less that 1. Preliminary simulations indicate a factor of 0.78.

Figure 3-18 (left) shows a scatter plot, 45° incidence angle T_BV (K) versus bed elevation, for the test area. The 45° data at V polarization is preferred since V is less sensitive to surface scattering than H pol, and 45° is close to the Brewster angle (the ice behaves as close to a blackbody as possible). The correlation, as already noticed in Figure 3-14, is evident, but significant scattering is also obvious. There are several reasons for the scattering but a major issue is temperature variations not corrected for in Figure 3-18. The influence of temperature is shown in Figure 3-18 (right), and the correlation is 0.77, i.e. very close to the factor 0.78 found from the simulations.

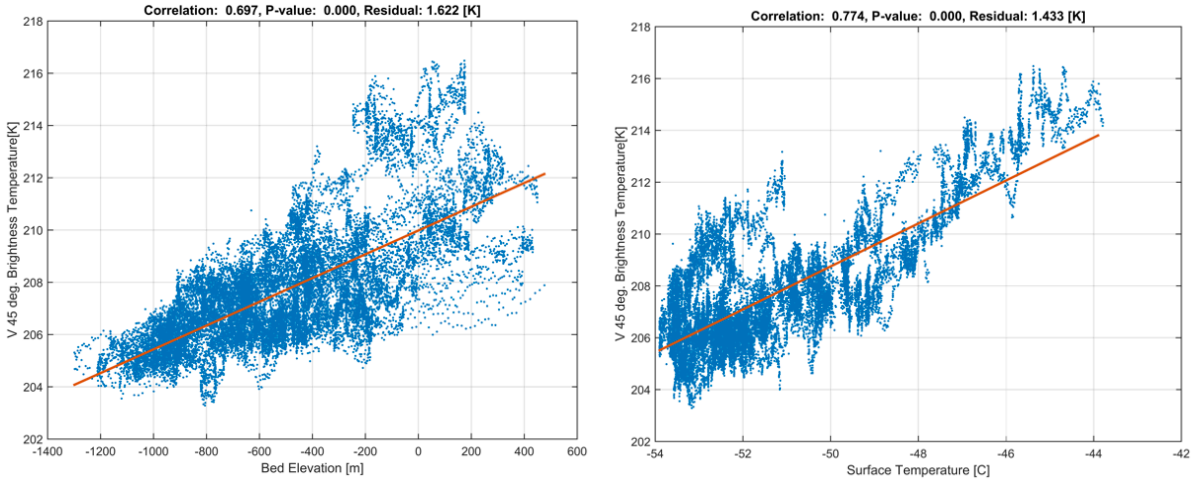

Figure 3-18: TBV versus bed elevation (left) and T_BV versus -10 m temperature (right).

Using this information, Figure 3-19 shows T_BV versus combined bed elevation and surface temperature variations. The result is quite good with a large correlation coefficient and modest scattering around the regression line.

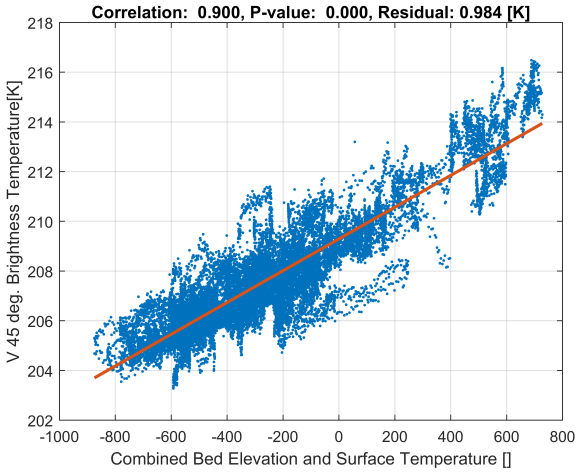

Figure 3-19: T_BV versus combined bed elevation and surface temperature.

Finding ice thickness using SMOS data

Based on the findings in the previous sections a procedure for finding bedrock elevation in the poorly known parts of Antarctica can be outlined:

- take 1 year averaged SMOS TBV, 45° incidence
- correct for -10 m temperature
- correlate with Bedmap in good areas around target area
- fix relation TB to ice thickness
- find ice thickness in target area
- find bedrock using surface elevation data

Figure 3-20 shows for the last time issues using data from the Concordia test area. The scatter plot of ice thickness versus T_B reveals that in this area 1 K change in T_B corresponds to 161 m ice thickness change, with a standard deviation of some 200 m. If this holds also for the target area, this is a significant improvement of the current map.

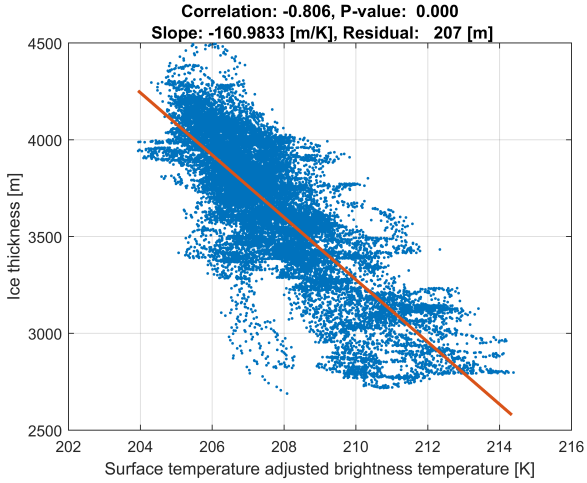

Figure 3-20: Ice thickness vs. SMOS T_B adjusted for surface temperature in the test area.

3.2.3 Experimental final product

Figure 3-21 shows an East Antarctica section of the Bedmap ice thickness map, where the red target area has been blanked out.

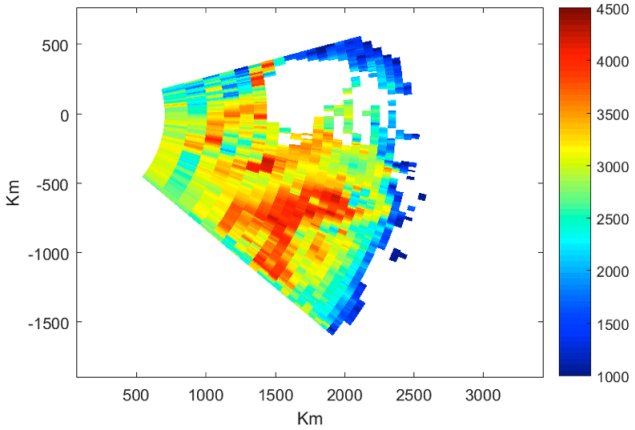

Figure 3-21: East Antarctica area Bedmap ice thickness (m).

Making the usual scatter plot (excluding the blanked out target area) of ice thickness versus T_B adjusted for surface temperature, results in Figure 3-22. Again a good correlation is seen, but the standard deviation has increased to some 400 m – still better than the original 1000 m.

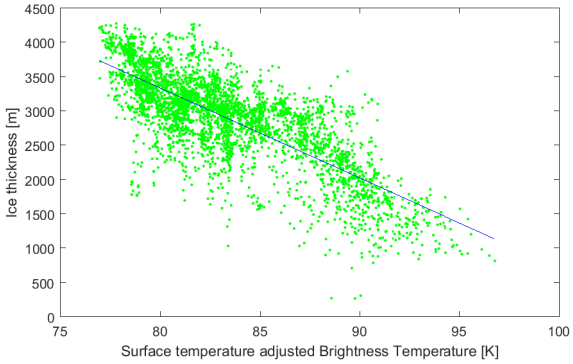

Figure 3-22: East Antarctica area ice thickness vs. SMOS T_B adjusted for surface temperature.

Using the slope found in Figure 3-22, fixing the level over the well known area, we can estimate the ice thickness in the target area, which then is patched into the map, see Figure 3-23. This map now has an accuracy better than 400 m all over.

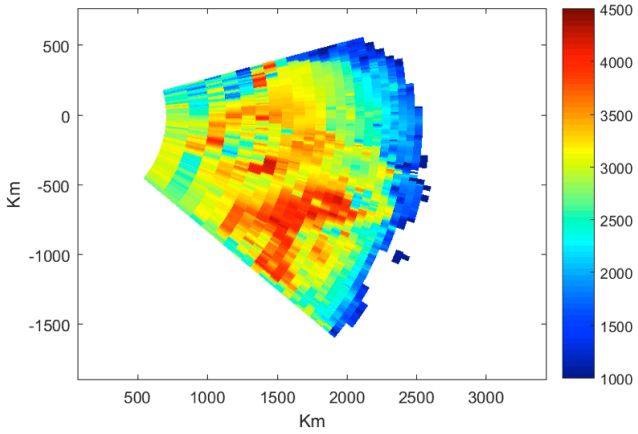

Figure 3-23: Bedmap ice thickness patched using SMOS data.

In conclusion, the 45° incidence angle vertically polarized L-band brightness temperature of the ice cap in Antarctica depends primarily on the physical temperature of the ice and the ice thickness. The physical temperature is known, hence the brightness temperature carries knowledge about ice thickness, hence bedrock elevation, since the ice surface is well known. A few, but significantly sized areas in Antarctica, have unknown bedrock elevation, and the current maps of bedrock can thus be improved. This is demonstrated in a target area in East Antarctica.

3.3 Case study n.3: Characterization of ice shelves

The microwave emissions in L-band from ice shelves are determined mainly by three quantities: the distance through the shelf which is covered by the electromagnetic (EM) wave, the transparency and strength of emission of the ice (determined by the loss factor/imaginary part of relative permittivity and physical temperature) as well as the surface/firn emissivity i.e. EM the fraction of upward emissions in the ice which enter the atmosphere (determined by the differences in relative permittivity at interfaces including the snow-air interface but also ice lenses inside the firn). The distance covered in the ice is in good approximation a linear function of the ice shelf thickness while the relative permittivity is mainly dependent on the ice temperature, density and the formation process of the ice determining the inclusion of impurities. Physical parameters with a potential influence on the SMOS measurements are: ice temperature and density profiles, strength of density fluctuations in the firn, the presence of marine ice and rifts going through the ice shelf.

Ice shelf specific processes influencing the physical temperature are special ice flow profiles (due to negligible basal strain) and average bottom heat fluxes, which can easily exceed the geothermal heat flux by a factor of 100. Marine ice freezing to the base of the shelf in some regions has not only an effect on the mechanical stability but has also very distinctive electromagnetic properties. The firn layer of ice shelves is governed by typically high accumulation rates and relative high air temperatures, which can lead to surface melt.

3.3.1 Theoretical understanding

The Emission Model

An incoherent multi layer ice and snow emission model with planar interfaces has been developed based on Maaß et al. (2013, and references therein). The implementation allows the use with around one thousand layers at reasonable computational costs while accounting for all interface reflections. The model has been adopted to ice shelves by implementing a base layer of sea water at -2.5 °C (the approximate pressure melting point of sea water) and if desired an intermediate layer of marine ice between water and the ice shelf.

References to used electromagnetic formulations for the different ice and snow types are listed in Table 3-2. Marine ice and Rifts are represented as areal concentrations and perturbations from the mean densities ρ are simulated as zero mean Gaussian distributed random noise with standard derivation σ. The total emission is derived as the mean of multiple simulations with different noise realizations. Three different temperature profile functions are used in combination with an exponential mean density profile. The input parameters of the model are:

- the surface temperature (T_s),
- the temperature profile function (one of three),
- the mean surface density (ρ_s),
- the firn thickness (ζ),

- the stratification factor (a_σ),
- the meteorological ice thicknesses (H),
- the area concentrations of marine ice (c_{MI}) and rifts (c_{RI}).

Table 3-2: Summary of used models/approximations

Property/Process	Method/Reference
Relative Permittivity Ice	Mätzler (2006)
Density dependence of Relative Permittivity	Tiuri et al. (1984)
Relative Permittivity Water	Klein and Swift (1977)
Relative Permittivity Marine Ice	Kaleschke et al. (2010)
Temperature Profiles	$T(z) = T_s + (T_b - T_s) * z/H$ (linear, #1) $T(z) = T_b + (T_s - T_b) \cdot \left(\frac{H-z}{H}\right)^{\frac{1}{3}}$ (Luckman et al. (2012), #2) $T(z) = T_b + (T_s - T_b) \cdot \left(\frac{H-z}{H}\right)^{\frac{1}{5}}$ (#3)
Mean Density Profile	$\rho(z) = 917 - (917 - \rho_s) \cdot exp\left(\frac{-z}{\zeta}\right)$ (in kg/m³, Bereiter et al., 2014)
Density Stratification in Firn	Method following West et al. (1996), fit to line E in Fig.7f of Hörhold et al. (2011): $\sigma_{QML} = 4.588 \cdot 10^{-12} \cdot \rho^5 - 1.612 \cdot 10^{-8} \cdot \rho^4 + 2.087 \cdot 10^{-5} \cdot \rho^3$ $-1.222 \cdot 10^{-2} \cdot \rho^2 + 3.054 \cdot \rho - 201.3$ $\sigma = a_\sigma \cdot \sigma_{QML} \rho_{total} = \rho + GAUSS(0, \sigma)$ (in kg/m³)

SMOS data

The used SMOS dataset is processed at the University of Hamburg based on the SMOS L1C version 620 (Mecklenburg et al., 2016). We use a fitting function from Zhao et al. (2015) to refine the characteristics of the multi-angular SMOS observations.

A comparison of SMOS Brightness Temperatures (T_B) with the distribution of marine ice beneath the Ronne-Filchner ice shelf from Lambrecht et al. (2007) gives indications for an increase in the SMOS intensity from marine ice (Figure 3-24). This increases our confidence that there is a contribution from deep layers of the ice shelf to the L-Band signal.

3.3.2 Retrieval approach

As the number of model input parameters exceeds the independent information in the measurements we are facing an ill-posed retrieval problem. To simplify this problem we separate the input parameters into two sets, namely surface + firn properties (ζ, a_σ, ρ_s, hereafter called surface properties) and internal + bottom properties (T(z), H, c_{MI}, c_{RI}, hereafter called bottom properties). The focus here will be on temporal variations in the SMOS measurements instead of the mean state

because, amongst other things, we have stronger confidence in the model for investigating the impact of changes in parameters than we have in the absolute values (likely biases).

The aim here is to retrieve which of these two sets is responsible of variations in the SMOS signal on a pixel by pixel basis. Two Monte Carlo setups have been used: varying the bottom properties on reasonable ranges while using constant values for the surface properties and vice versa.

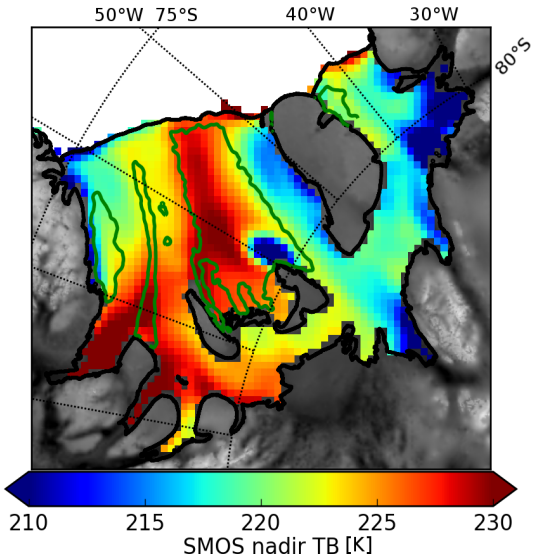

Figure 3-24: SMOS near nadir T_B (<40°) from 2010 to 2015 at the Ronne-Filchner Ice Shelf region with contour of significant amounts of marine ice (Lambrecht et al., 2007). In addition the grounding and coast lines (black) from the MODIS Mosaic of Antarctica project 2009 and the land topography from Bedmap2 (shades).

Figure 3-25 shows that the relation between modeled TB^{v40} (v-polarization at 40°) and normalized polarization difference at 40° (hereafter called polarization, $Pol = \frac{TB^{v40} - TB^{h40}}{0.5(TB^{v40} + TB^{h40})}$) is different for variations in bottom properties (green) and near surface properties (blue). The main influence of bottom properties on the signal are changes in non-polarized emissions within the ice while surface properties have an influence on the signal due to an intensification or reduction of interface reflections, which modulate the h-polarisation stronger than the v-polarisation. These different signatures are exploited in the following to identify the origin of observed variations.

SMOS T_B changes within the bounds shown in Figure 3-25 are judged to be in agreement with changes surface (blue dashed lines) and bottom (green dashed lines) properties. A linear color scale is assigned to ratios outside of these two intervals as shown by the inlet in Figure 3-25.

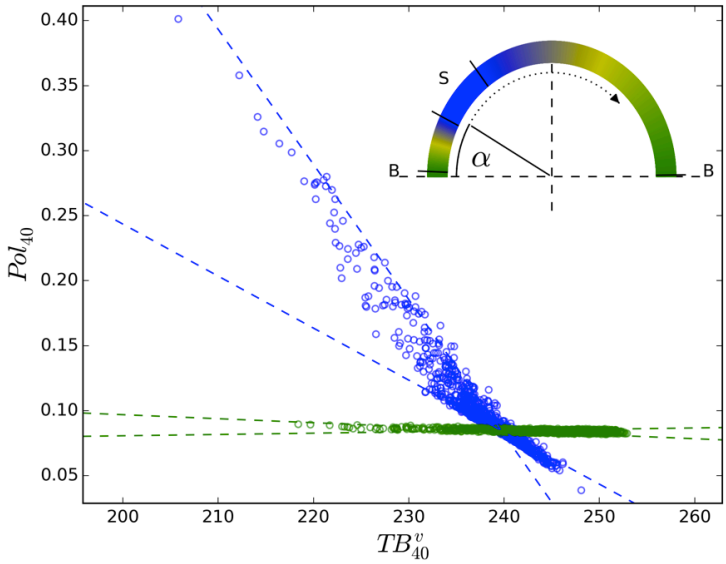

Figure 3-25 Model results (points) varying only near surface parameters (blue) or bottom parameters (green) with 2.5 and 97.5% quantiles of repeated orthogonal regressions on six randomly chosen points (dashed lines). The inlet illustrates the definition of a color scale based on the quantiles.

The derived estimate of origin is complemented by an evaluation of the strength of variations R_{max}. In order to relate changes of TB^{v40} and polarization we use scaling the factors $SC_{TB} = 0.1K$ and $SC_{Pol} = 0.0008$, respectively. In regions with large R_{max} the observed changes are much larger than those of a predominantly stable reference area (Dome C). To avoid direct observations of surface melt/wet snow we exclude the summer month before deriving yearly means.

3.3.3 Experimental final product

A brief Overview

The general picture of the product is as expected (Figure 3-26): while there are areas of surface and bottom driven variability at ice shelves, surface processes are dominating inland. However, there are grounded areas with detected bottom changes, e.g. at the Antarctic Peninsula. Variations in SMOS are small in central Antarctica compared with ice shelves in general but the more northern ones (Larsen-C, Amery) in particular.

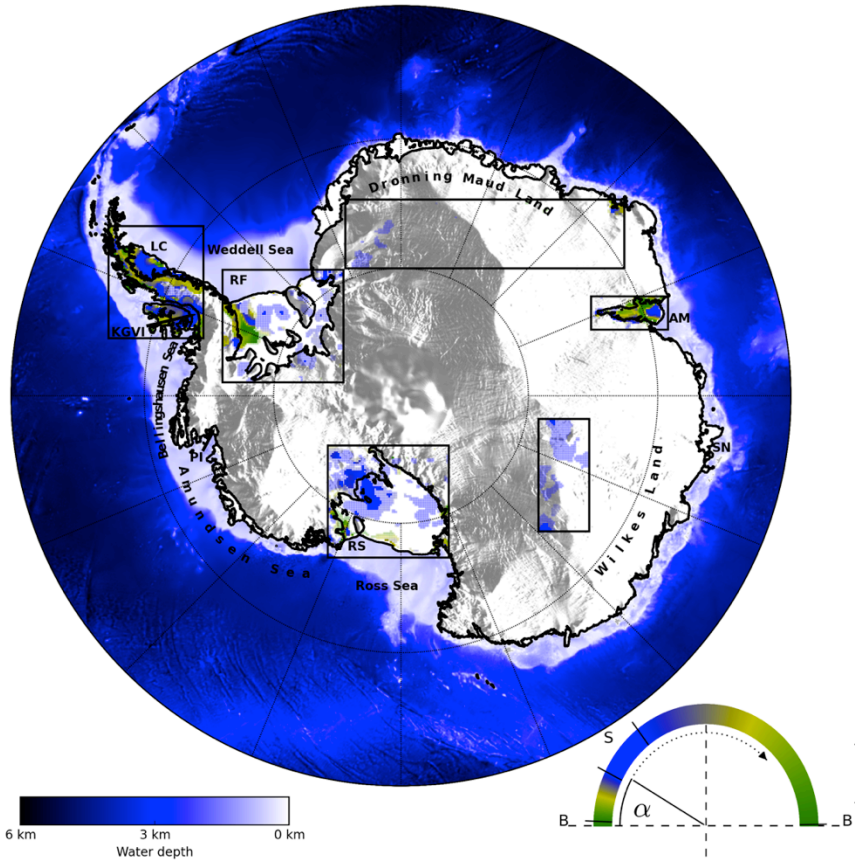

Figure 3-26: Locations of six study regions (frames) with estimates of the origin of SMOS variations for Rmax> 6 (pale colors) and Rmax> 10 (intense colors). Grounding and coast lines (black) from MODIS Mosaik of Antarctica 2009 as well as surface (shades) and sea floor topography from Bedmap2.

The Ronne-Filchner ice shelf

The combined estimate in Figure 3-27 shows strong variations of SMOS measurements in the eastern part of the Ronne ice shelf. The strongest variations coincide with signals driven by bottom changes (green) or by a combination of bottom and near surface changes (yellow). Estimated surface driven changes are often changing the location from year to year and have typically smaller amplitude than bottom driven variations (making them frequent in the yearly but less frequent in the combined estimates). Strong variability in SMOS often coincides with the edges of marine ice fields (Figure 3-27). This can be explained by the fact that a thin marine ice layer increases the SMOS sensitivity to bottom melt/accumulation as it is in-transparent for SMOS after 1 to 2 meters while a change in meteorological ice thickness of two meters would have only a minor effect on the signal.

The major oceanic flow for the western side of the ice shelf (black dashed line in Figure 3-27 and Figure 3-28) coincides well with regions of strong, mostly bottom driven variability in SMOS measurements until it reaches the Korff Ice Rise. Linking the water inflow to the observed variability would imply that the bottom mixed water layer of warm and saline water is able to influence the ice shelf base in this area with around 400 m of cavity height.

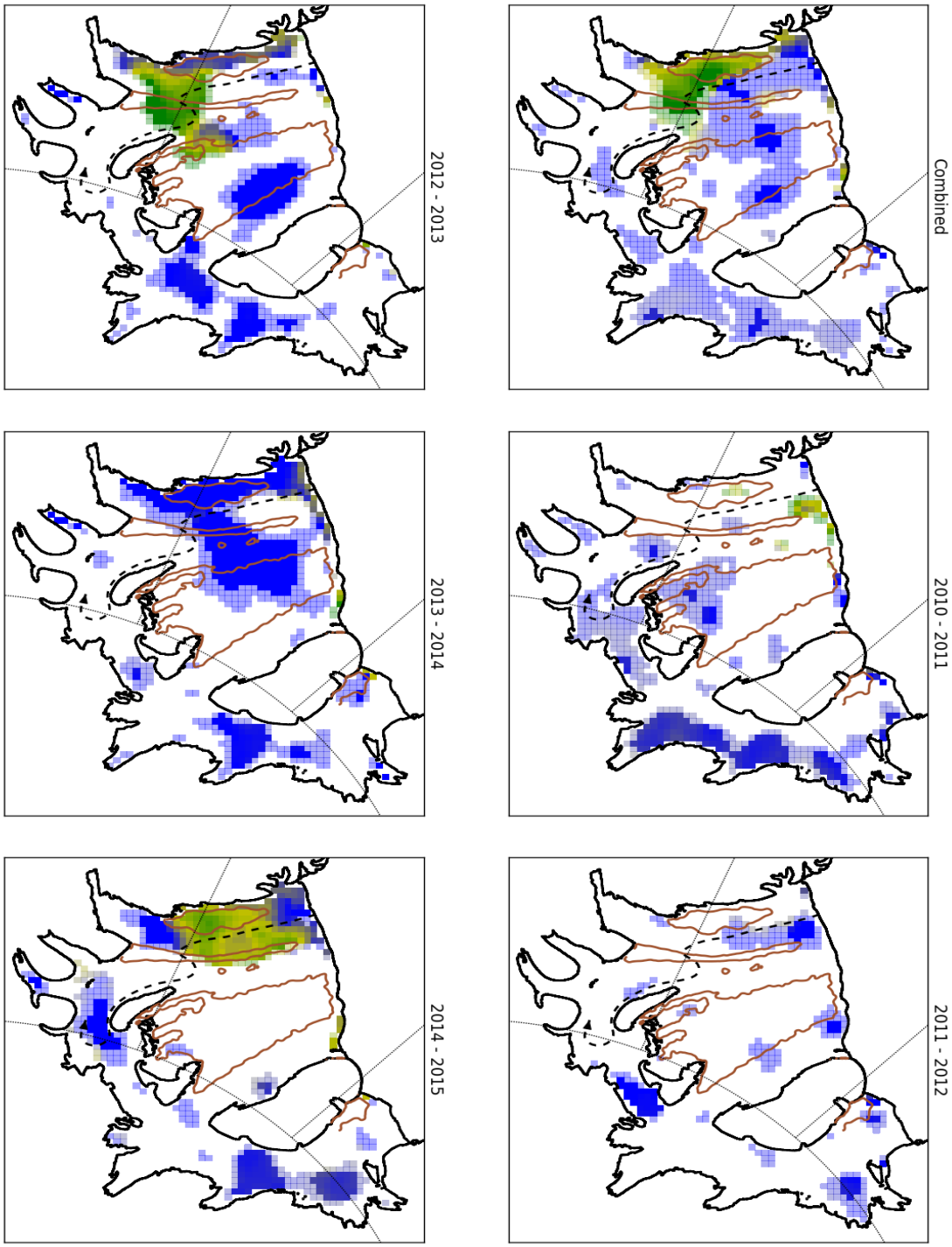

Figure 3-27: Estimate of the origin of SMOS variations at the Ronne Filchner ice shelf (ice shelf only) combined for the whole period (R_{max} > 10 (intense colors), 10 > R_{max} > 6 (pale colors) and 6 > R_{max} (white)) and for each yearly mean to yearly mean difference individually (R_i > 6 (intense colors), 6 > R_i > 4 (pale colors) and 4 > R_i (white)). Brown lines enclose areas with significant amounts of marine ice (Lambrecht et al., 2007) and black dashed line shows one major oceanic flow pattern (Nicholls, 1997).

The area of internal/bottom driven variations (green) in Figure 3-28 has an elongated extension towards the central Ronne ice shelf north of the Korff ice rise which coincides with the 770 m sea floor topography contour. Even though this extension is at about the resolution of SMOS we do think that it originates from a warm and saline intrusion of HSSW into this region between 2012 and 2013.

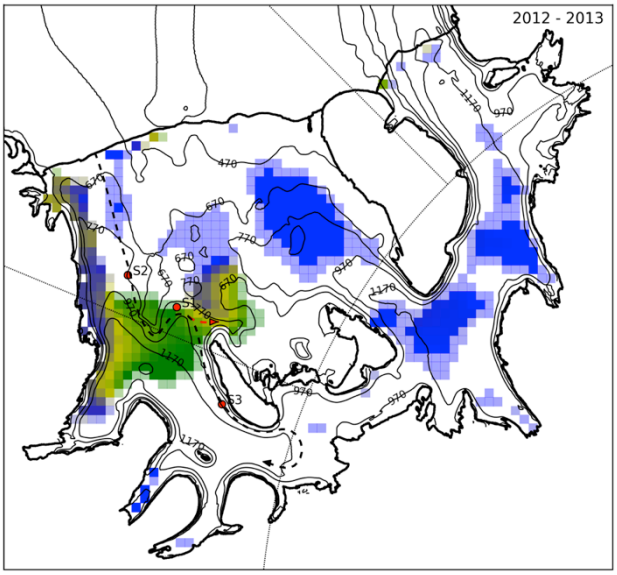

Figure 3-28: Origin of changes in SMOS between 2012 and 2013, $R_i > 6$ (intense colors), $6 > R_i > 4$ (pale colors) and $4 > R_i$ (white)) but with contour lines showing Bedmap2 sea floor topography [m below sea level]. Note the irregular spacing of the contour lines. Red dots denote the locations of hot water drilling stations (Site 1 to 3).

The HSSW enters the Ronne cavity as geostrophic flow which is situated below could and fresh Ice Shelf Water (ISW) on the sea bed. Figure 3-28 shows that there is a depression in the sea bed to the south east from the mean flow pattern described in the literature (Nicholls, 1997). Depending on the depth and thickness of the HSSW flow in this region, parts of it might follow this depression and promote melt at the base of the ice shelf (short red arrow in Figure 3-28). A hot water drilling station from 1991 was less than 50 km upstream of the possible flow divide (Site 1). The mean pycnocline at this site was at a depth of 700 to 750 dbar (Nicholls and Jenkins, 1993), just above the depth below sea level of the depression of 760 to 800 m (Bedmap2). The flow of HSSW into the Ronne cavity has a strong seasonality (Nicholls et al., 2009) leading also to a seasonal cycle in the depth of the thermocline of at least 130 m at drilling Site 3, about 200 km downstream of the possible divide (compare Fig. 2 in Nicholls (1997) and Nicholls and Østerhus (2004)). At the upstream Ronne depression (Site 2; Nicholls, 1996) the seasonality is 50 to 60 m. The topographic gradient at Site 2 is much smaller than at Site 3 (Figure 3-28), which can be associated with a widening of the flow explaining the reduced amplitude of the seasonality in thermocline depth.

The combination of thin marine ice and a variable oceanic flow, able to melt marine ice if present or allow the formation of it if absent, is a conclusive explanation of the SMOS signal. If this is the case we have been able to link satellite observations to oceanic flows in an ice shelf cavity for the first time.

The Amery ice shelf

The Amery ice shelf is about 5 to 10 degrees north of the Ronne ice shelf which is one of the reasons why it is much more often subject to surface melt. It is therefore reasonable that the Amery ice shelf shows strong surface driven fluctuations. However, there is an area of mostly bottom driven variability in its southern half, which has been discussed to be an area of marine ice aggregation (Figure 3-29). The north eastern part of the ice shelf is also facing bottom freezing but is not identified as such by the SMOS product. This can be explained by the already large amount of marine ice in this region (Fricker et al., 2001) diminishing the SMOS sensitivity. At the same time could surface processes overlay a potential bottom signal.

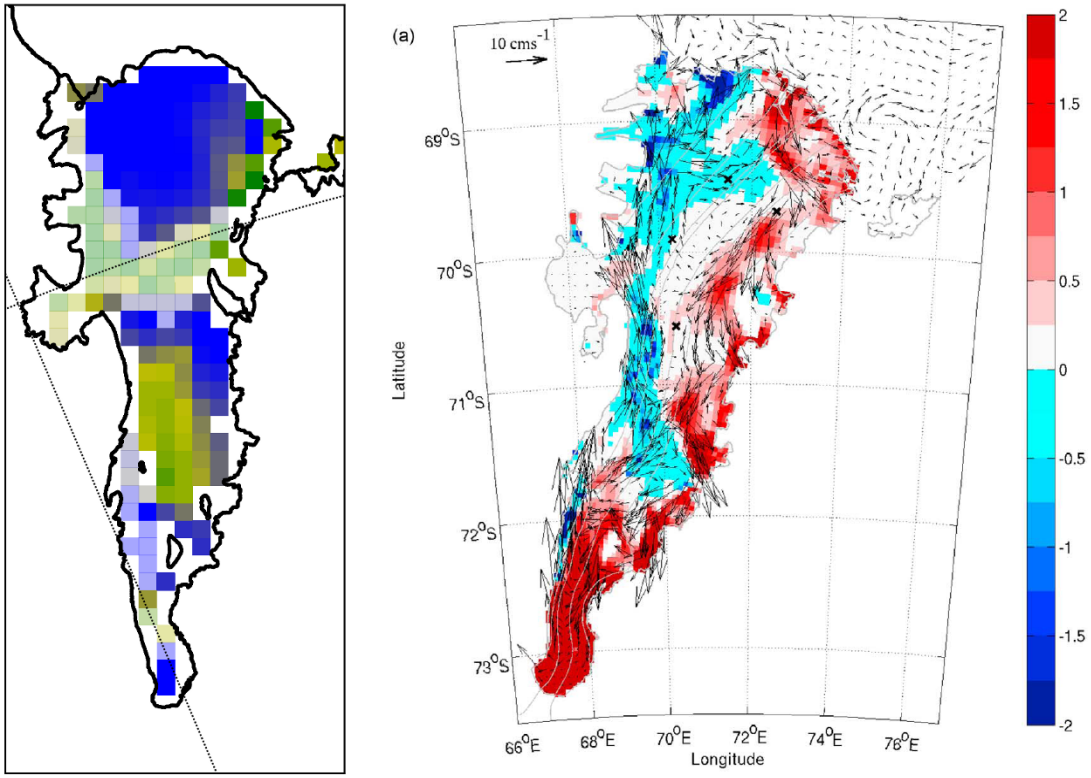

Figure 3-29: Left: estimate of the origin of SMOS variations at the Amery ice shelf (R_{max} > 10 (intense colors), 10 > R_{max} > 6 (pale colors) and 6 > R_{max} (white)). Right: annual averaged model estimate of melting (positive; m ice year^{-1}) and freezing (negative) superimposed with depth average currents. Figure from Galton-Fenzi et al. (2012).

Validation with surface events

There are basically two events at the Antarctic Peninsula which show strong widespread decline in SMOS T_B while at the same dates the near surface air temperature is exceptional high (Figure 3-30). This concurrency along with the lasting impact on the SMOS T_B strongly suggests one explanation: surface melt leading to the formation of pronounced ice structures. These two events are utilized here to validate the identification of surface driven changes. For this purpose we use the differences in mean T_B intensity and polarization fields based on ten-day means from before and after the events. Selection of validation samples is also based on amplitude of observed changes and location.

Figure 3-31 shows the changes in T_B against the changes in polarization for both surface events. The model predicts changes in surface properties to influence the signal with a polarization to T_B ratio somewhere between the two blue dashed lines. This area contains only 36% of all validation points while 94% are at least closer to the surface class than to the bottom class. Another 0.5% of the validation points show a signal predicted for bottom changes (between the green dashed lines). The mean polarization to T_B ratio of all validation points coincides with the lower bound of the predicted surface signatures.

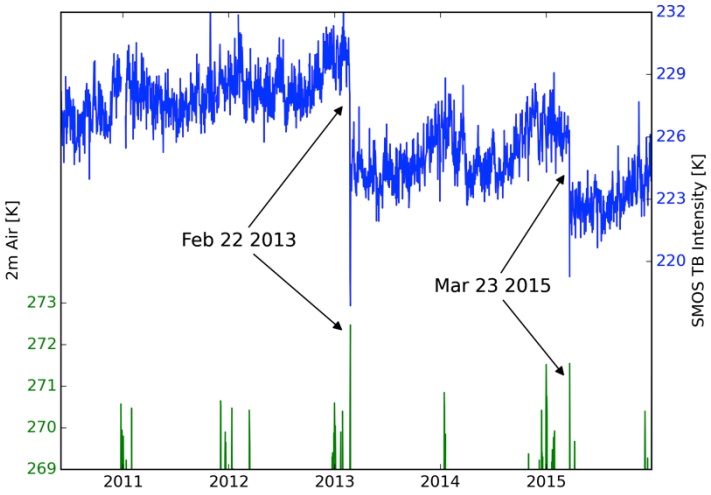

Figure 3-30: Two meter air temperature from NCEP reanalysis 1 (left, green) and SMOS T_B intensity (right, blue) for one location on the Antarctic Peninsula.

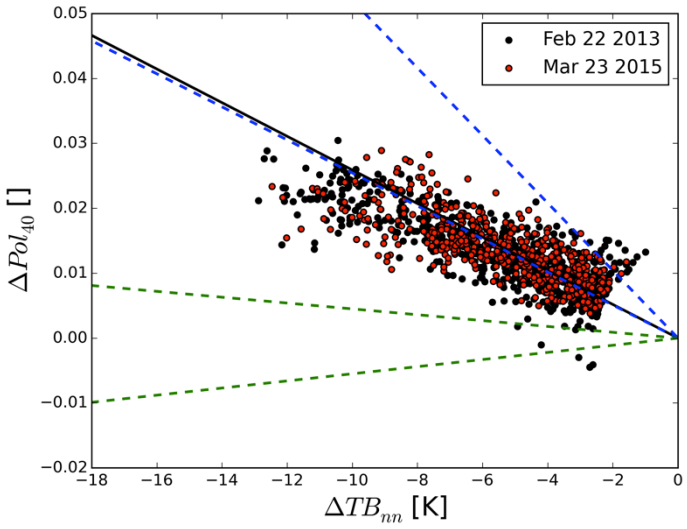

Figure 3-31: Changes in SMOS intensity and polarization by the two surface events highlighted in Figure 3-30 with mean direction of all observations (black line). For comparison, range of model predictions of surface (blue) and bottom (green) intensity to polarization ratios (dashed lines).

Most model runs of the surface setup (blue dots in Figure 3-25) are well represented by the lower bound while much fewer runs (having very small surface densities which is not expected at the Antarctic Peninsula; not shown) determine the upper bound. This validation study suggests that the model agrees well with observations on the mean influence of surface events but does not cover the full range of variability.

3.4 Case study n.4: Characterization of surface processes

The state of the surface is essential to understanding and predicting the surface energy and mass budgets, which are two key nivo-meteorological variables of interest for the study of the climate and as a contribution to the sea level of ice-sheets. Snow properties such as grain size, wetness, density, and roughness are linked to air temperature, surface wind, precipitations, etc. SMOS observations could help to detect fresh snow in order to supply information about precipitations, to follow variations in roughness linked to wind, as well as monitor melting periods (number of melting days per year, duration, starting date, etc.). Thanks to the large penetration depth at L-band, SMOS observations could detect whether melt is deep and impacts on snowpack stability, contrary to higher microwave frequencies sensitive to the first meters of snowpack only.

A first preview of SMOS observations has shown that two main regions can be identified which are characterized by different kinds of snow and processes. The first is the internal part of the continent, which is always dry. The L-band brightness temperature (T_B) is very stable, and any small variations observed could be interpreted as changes in the surface state (snow density, surface roughness, etc.). The second region is the wet snow area, which is located mainly along the coast and on ice-shelves. Here, the surface state is affected by seasonal melting events that considerably influence the snowpack structure. In the following, both areas are explored.

3.4.1 Theoretical understanding

3.4.1.1 Dry snow area

On the Antarctic Plateau, the six years of Earth monitoring from the SMOS satellite showed the stability of L-band T_B. At Dome C over the period June 2010 – June 2016, mean SMOS T_B at 52.2° of incidence angle is 217.3 K ± 0.7 K and 179.9 K ± 1.5 K in vertical (V) and horizontal (H) polarization, respectively. Thus, any small variations observed could be interpreted as changes in the surface state. A detailed analyse has been performed at the Dome C test site and presented in Leduc-Leballeur et al. (in revision). The results are summarised in the following.

From November 2014 to March 2015, the slow increase in T_BH concomitantly occurred with a decrease in surface snow density (Figure 3-32). During this period, low wind speed allowed the hoar presence and accumulation of light snow. Around March 20, 2015, an abrupt decrease in T_BH (higher than 5 K at 52.5° of incidence angle) was observed corresponding to clear increase in surface snow density. Strong wind was also observed, which could have compacted or removed the light snow presents at the surface.

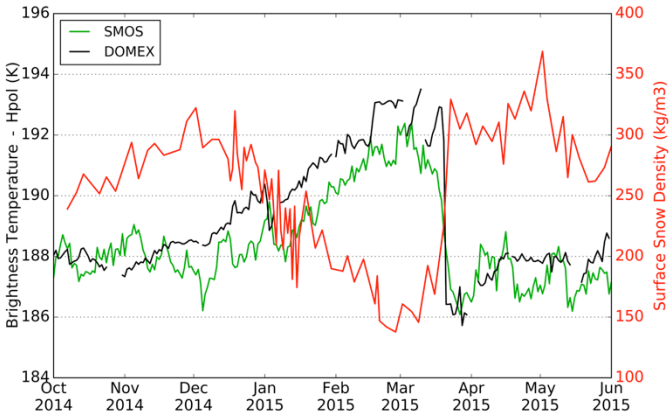

Figure 3-32: T_BH with SMOS at 52.5° incidence angle (green) and DOMEX at 42° (black), and surface snow density in situ measurements (red) at Dome C, Antarctica from October 2014 to May 2015.

The snow emission model WALOMIS (Wave Approach for LOw-frequency MIcrowave emission in Snow, Leduc-Leballeur et al., 2015) based on the wave-theory was used to investigate the snow properties change that could explain these exceptional variations (West et al., 1996, Tsang et al. 2001). As a first step, the simulations only considered the variations of surface snow density measured at Dome C. A good agreement is obtained between simulations and SMOS observations for the first part of the period, suggesting that T_BH is affected by change in surface density. However, to completely reproduce T_BH variations, it is necessary to account for the variations of the surface layer thickness. Daily measurements of the surface elevation have been used to estimate the variation of the layer thickness. The simulations taking into account both snow density and layer thickness at the surface showed very satisfying agreement with the observations.

These results confirmed that T_BH is influenced by the snow properties of the first centimeters in spite of the large emission e-folding depth at L-band (several hundreds of meters). More importantly, this showed that the thickness of superficial layer is an important factor, which is a specific feature of the low frequency that results from interference phenomena. Radiative transfer theory does not predict such a dependence to the thickness and is in principle inadequate to describe layers thinner than the wavelength. We therefore recommend to use the wave theory approach in the lower part of the microwave domain.

The causes of the changes at the snow surface that resulted in the exceptional T_BH changes are complex and partially elucidated here. They are linked to an exceptional hoar formation during the summer as well as to snow accumulation. Both were made possible by weaker-than-normal wind that prevailed for long periods before March 20, 2015. A layer of light snow likely grew until its thickness became sufficient to be detected at L-band.

The extension of this study to the whole continent is an avenue but could be challenging because of the lack of in situ measurements. Indeed, L band T_BH is sensitive to snow density and thickness of surface layer, but these two parameters are strongly linked/mixed. Thus, it is difficult to separate two effects. However, useful information on changes in snow surface could be obtained for climatic

studies, such as following a trend or identifying specific events. Deeper analyses are needed in order to find the best way to retrieve useful information over the whole Antarctic ice sheet.

3.4.1.2 Wet snow area

Remote sensing by microwaves is sensitive to surface melting. Indeed, the onset of melting produces a marked rise of T_B that is caused by moisture in the near-surface firn due to the high dielectric absorption of liquid water. Several efficient algorithms have been developed to detect these changes in Greenland (e.g. Abdalati and Steffen, 1997) and in Antarctica (e.g. Ridley, 1993; Zwally and Fiegles, 1994; Torinesi et al., 2003). We have exploited these studies in order to set up a robust algorithm for the detection of the melt in Antarctica from L-band SMOS observations and generated a surface melting product over the continent.

3.4.2 Retrieval approach

Although the emissivities of wet firn at H and V polarizations are nearly equal, the emissivity of dry firn at H polarization is significantly lower than at V polarization. Therefore, H polarization is used, because the increase in T_B with melting is expected larger than at V polarization.
Zwally et al. (1994) and Torinesi et al. (2003) suggested a criterion to detect melting day from T_B at 19 GHz. Here, a similar retrieval approach is used for 1.4 GHz SMOS T_B. Melt induces large increases of T_B and an annually and regionally varying threshold can be calculated. All values of T_B above the annual mean plus this threshold are associated with melting. This threshold is proportional to the standard deviation of the signal in order to take into account the spatial variability of its amplitude. Thus, the threshold T above which a T_B value is considered to be a melt signal is the mean M plus N standard deviations σ:

$$T = M + N\sigma$$

For each year from 2010 to 2015, the annual mean of brightness temperature at horizontal polarization is calculated between 1 July and 31 June in each grid point. This annual mean allow to take into account the interannual variability of the signal. But, it is also essential to remove the bias introduces by the high values typical of melting, which do not reflect average values of unaffected period. Thus, these melting events are filtered out by eliminating values more than 10 K above the annual mean. This process is repeated two times. The first time, the mean is calculated using all the values (without any filter); then strong melt signals are filtered out and the calculation is performed a second time. Thus M and σ are calculated from the obtained time-series vary for each year and each grid point. The value of N is a constant and the selected value is N = 2.5 (Torinesi et al., 2003; Picard et al., 2006). This optimal value is determined by an analyse based on daily air surface temperature (Torinesi et al., 2003) and its typical of outliers detection. N had been adjusted to detect all and only the real melting days, as possible.

The algorithm is designed to detect individual melting events for every grid points and each day. It returns two possible values: 1 for the status melted, or 0 for not-melted. Figure 3-33 shows an example of melting detection from 2010 and 2016 in the East of Antarctic close to the Amery ice-shelf. The threshold separately defined for each year (black lines) allows a good detection of the main seasonal peak of T_B.

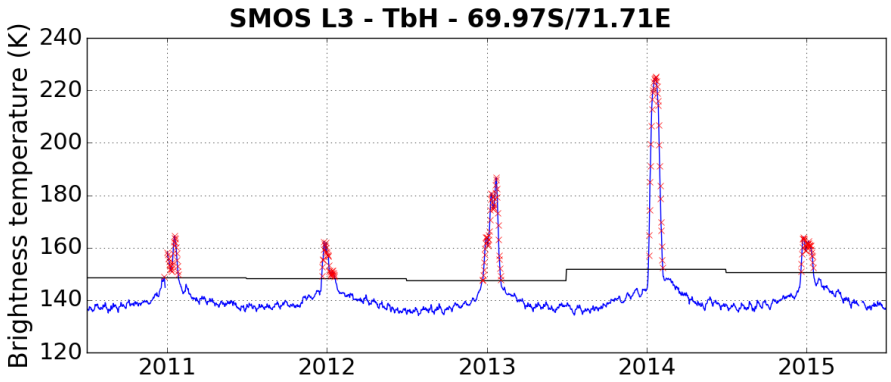

Figure 3-33: T_B at H polarization (K, blue) from SMOS at 69.97°S, 71.71°E from July 2010 to June 2015. Threshold defined by the algorithm is represented in black and the detected melting days are in red stars.

Due to the lack of in situ measurements a detailed validation is difficult. However, a possible way to check the reliability of the melting detection by SMOS is to perform a comparison with another product of melting detection by microwave satellite. Picard and Fily (2006) retrieved a dataset of daily surface melting in Antarctica from passive microwave radiometer observations at about 19 GHz (available on http://gp.snow-physics.science/melting/). The product includes the melted/not melted status of every pixel on the reduced Southern stereographic polar grid for every day since 1st April 1979 with a spatial resolution of 25 km but the underlying data are at about 60 km resolution. The temporal resolution is 1 day (2 days before 1988) and records are almost continuous since 1979. The current version of product provides maps up to 2015, which permits a comparison of 5 years with the SMOS product (from 2010 to 2015).

From SMOS product and 19 GHz product, it is possible to retrieve the beginning, ending and duration of melting period during each year (one year begins the 1 July of year N and finishes the 30 June of year N+1). Figure 3-34 shows an example of duration of melting obtained with both products for the 2012-2013 season. A significant correlation is observed each year between surface melting duration from SMOS and 19 GHz products. However, some differences are observed between both products, which could be explained by the difference of penetration depth of two frequencies. Indeed, a small melting event, which produces little water, may remain undetected at 1.4 GHz although it causes enough absorption at 19 GHz. In contrast, at the end of the season, the penetration depth at L-band is so large that the signal is sensitive to liquid water at depth, event if coarse-grained snow (or refrozen snow) are present and act as a shield for 19 GHz. As a consequence, the differences between both products may be very useful to improve the characterisation of the seasonal melting events. For example, if 19 GHz product shows a melting period whereas not SMOS product, it is likely that melt is

weak. But, if SMOS product shows a longer melting period than 19-GHz product, we can suggest that melt affects the inner part of firn and the melt event is strong.

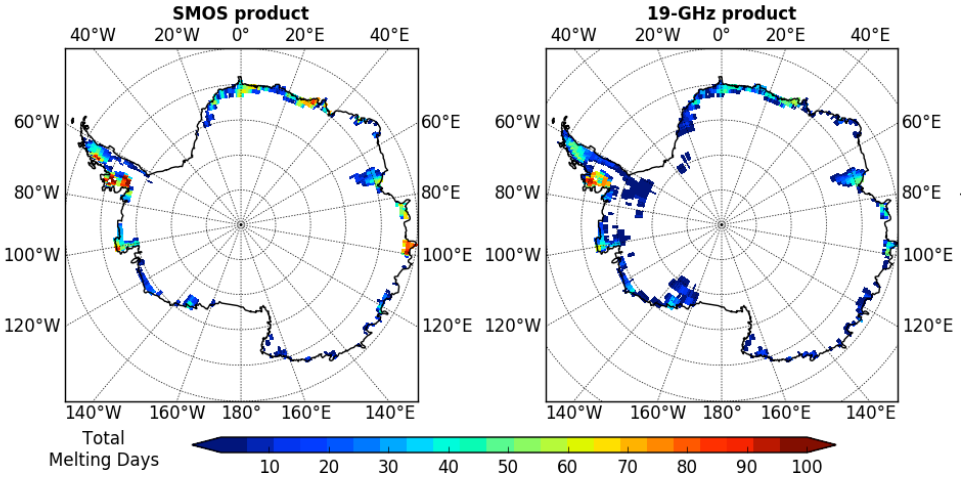

Figure 3-34: Maps of duration of melting period detected by SMOS (right) and 19 GHz (left) melting products for the 2012-2013 season.

3.4.3 Experimental final product

The product "Occurrence of Surface Melting" includes the melted/not melted status of every pixel each day, as well as the mask which excludes the ocean as well as areas never experiencing melting and areas above 1000m. The main characteristics of this experimental product are listed in Table 3-3.

The product is estimated from the SMOS Level 3 product (Kerr et al., 2013 Al Bitar et al., 2017) distributed by CATDS (Centre Aval de Traitement des Données SMOS; http://www.catds.fr/). It is geolocated on an Equal-Area Scalable Earth version 2.0 grid (EASE-Grid2; Brodzik et al., 2012), with an oversampled resolution of about 628 km^2, which is distorted in the polar regions (around 100 x 6 km^2 as latitude x longitude). The daily-averaged T_BH at 52.5° of incidence angle was used and the occurrence of surface melting product is provided daily from July 2010 until June 2015. The coverage is limited to Antarctica.

Table 3-3: Characteristics of the "Occurrence of Surface Melting" experimental product.

Spatial coverage	Antarctica
Spatial resolution	The global EASE2 grid (628 km^2 by pixel)
Temporal coverage	2010-2015
Temporal resolution	Daily
Parameter	the melted/not melted status

4 Conclusion and recommendations

The work performed during the CryoSMOS project highlighted the potential of SMOS observations to provide useful information about Antarctica. SMOS T_B spatial and temporal signature was observed in Antarctica, was first of all explained from a theoretical point of view by using microwave emission models. In particular dependency on physical parameters that mainly affect the microwave emission at L-band was identified. Staring from this, four research SMOS derived products have been developed:

- internal ice-sheet temperature,
- ice thickness,
- indicator of the origin of ice-shelves variability,
- surface melting occurrence.

These products are considered as scientific products (contrary to operational products which are produced on a daily basis) that need to be better assessed by further investigations. They are available at CATDS (http://www.catds.fr/Products/Available-products-from-CEC-SM/CryoSMOS-project) and any updates on data sets could be submitted. It is strongly recommended that referenced papers will be added, when available, to support the research activities of the project.

The experimental products developed could be used for various topics of study and/or open the door for other advanced products and applications.

4.1 Benefit and impact to the scientific questions

The internal temperature is a key parameter for the ice sheet dynamics and knowing its value is fundamental to better understand the changes in ice sheet mass balance and dynamics. Ice processes, such as the ease of the ice internal deformations or the rate at which the ice flows across the base, are strongly related to the temperature profile and in turn influence it. The temperature profile product can also be relevant to detect the presence of aquifers at the bottom part of ice sheet. Finally, another application for temperature profiles is the paleoclimate studies, in particular to identify the location of oldest ice, which is essential to the knowledge of paleoclimate. Is should be point out that, up to now, this information is available in only few available bore holes and existing and future satellites are unable to derive it.

The ice thickness estimated from SMOS observations is scientifically very interesting. Firstly, it confirms that the L-band T_B is so well modulated by ice thickness (which was not expected a few years ago). Secondly, this provides an alternative thickness measurement method, with its own, unique error issues, to compare with the classical and more fundamental radar measurements. Thus, despite a low accuracy, SMOS product gives useful information in the few area of Antarctica, which are not covered by measurements.

SMOS observations allow for the first time to observe changes at the basal interface of ice shelves from space because of the very large penetration depth (or better called emission depth) of microwave radiation at 1.4 GHz. This is a unique new information about ice shelves, in particular about their variability. Indeed, the change map from the CryoSMOS experimental product showed dramatic changes observed over Larsen C and King George VI, which call for immediate coordinated research action.

Surface melting occurs every summer on Antarctic coasts. Although surface melting has a minor overall contribution to the mass balance (Ohmura et al., 1996), it is of interest for climatology: surface melting extent and duration are climatic indicators related to surface temperature and the radiative budget. The Surface melting SMOS product can improve the survey of extent and duration melting events with respect to higher frequency radiometers at the scale of the continent, as well as in specific areas such as the Peninsula, Ross or Ronne ice-shelves. Moreover, benefits of SMOS observations also come from its large penetration depth, which could detect whether melt is deep and impacts on snowpack stability, contrary to higher microwave frequencies limited to the first meters of the snowpack.

4.2 Limitations of the experimental products

Although the new research products can be useful to address several topics, it is important to remember that they suffer from some limitations. Generally, due to the sparse coverage of the in situ measurements in Antarctica linked to the limited possibility of operating in such a harsh environment, the validation of products is very difficult. For example, there are just few ice cores available in the Antarctic ice sheet to evaluate the reliability of the retrieval temperature profiles. However, the drilling of boreholes is a very expensive activity and it is not expected/planned that the activity will be more intensive in a near future except for the hole will be drilled for paleoclimate studies. In the same way, any measurements are currently available to validate the ice-shelves variability product and the surface melting detection product.

Some limitations also come from methodology and specificity of L-band frequency. Thus, the algorithm to retrieve the temperature profiles product is not able to provide estimation over the whole ice sheet, because the method is based on the Robin model, which is not valid in some large areas where the ice advection at the bottom is not negligible. Moreover, L-band is sensitive to the first 1500-2000 m of the ice sheet although the ice is deeper in many places. Temperatures retrieved for in depth are then affected by a higher the uncertainty.

About ice-shelves, the algorithm allows to detect the origin of dominant changes, i.e. at the surface or at the bottom. But it should be noted that in some case, the dominant signal could mask a not negligible secondary signal. For example, the six years of SMOS observation reveals significant year to year variability at the Ronne-Filchner and Amery ice shelves, which point to bottom changes.

Nevertheless, possible bottom changes at the Antarctic Peninsula (Larsen C and King George VI ice shelves) are possibly masked by strong surface changes, which dominate the signal. Step-wise drops of the intensity after peaks of high air temperature have been observed on the land of the Antarctic Peninsula.

4.3 Outlooks and recommendations

Several outlooks can be proposed to overcome the above limitations in future and to transfer the outcomes of the CryoSMOS project into future scientific activities. The great potential of SMOS observations over the cryosphere can be continued to exploit on the one hand to develop and improve the current work on Antarctica, and on other hand, by using results and methods obtained to study new area of the cryosphere, such as Greenland and other frozen areas.

From a methodological point of view, a clear recommendation to perform improvements in Antarctica would be to explore the potential of multi-sensor approaches, as well as, to put strong effort on the collection of in situ measurements.

A plan for a potential scientific strategy can be elaborated for various activities.

- Short-term activities:

  Internal temperature of ice sheet:

  The next step is to extend the validity of product to a large proportion of the continent. Currently, the application is actually restricted to the areas where the Robin's model is valid. For that, a strong connection with the glaciological community should be build to extend the Robin's model or to develop a more complex model. This activity is quite challenging since the structure of the ice and its dynamic gets more complex than in the middle of the continent. The validation of such model needs in situ measurements; It is expected that further information should be available in the forthcoming years thanks to the drilling activities that will be carried out over the continent for paleoclimate studies. Moreover it is also recommended to explore the synergy to other EO sensors (GOCE, Cryosat2, IceSat) in order to improve our knowledge on Antarctica mass balance and improve the cooperation to other international initiatives (e.g. IMBIE project). The gained knowledge, developed tools and datasets shall be provided to ice sheet flow, mass balance and climate modellers in order to exploit their potential to improve predictions of current and future ice sheet and climatic changes including the estimation of sea level rise contributions.

  Surface melting detection:

  Comparison between surface melting detection from SMOS and from SSMI (at 19-GHz) showed a possible complementarity of these frequencies due to the difference of penetration depth. Indeed, the 19-GHz frequency with a penetration depth of about 20 centimetres is strongly sensitive to changes close to the surface. On the contrary, the 1.4 GHz frequency with a penetration depth of several hundred metres in the snowpack is less sensitive to the surface. Therefore, it could be very useful to exploit in parallel both frequencies to improve the characterisation of the seasonal

melting events. Comparison to active sensors, very sensitive to wetness, should be also considered. For climate applications, the detection of surface melting events should become operational or at least updated on a regular basis at CATDS. A near-real time product can be implemented at CATDS if a particular demand is clearly identified, such as continuous monitoring and assimilation into models in support of climate and weather forecasts.

- Further outlook:

Greenland

Greenland is clearly a hot topic in climate science as it rapidly responds to climate warming. The context of Greenland is more complex that in Antarctica due to, among other considerations, the important presence of water. However, considering the potential of SMOS data as demonstrated over Antarctica, a particular attention must be put on Greenland. The surface melting can easily be detected and has proven to be of interest and used to discuss climate change. The work developed for Antarctica should be tested and adapted to this specific case. The internal temperature is a more difficult task than in Antarctica. A few ice drills done in Greenland can be used to adapt the methodology. The use of other sensors (AMSR sensor family) at different microwave frequencies can help to better assess the processes that occur in the Greenland ice packs.

Ice shelves stability

An interesting signature at L-band has been observed over the Ice shelves. For instance, SMOS TB showed a constant decrease since 2010 over the Larsen C ice shelves. The observations should be extended to 2017 to confirm the observed trend and to link it to climate variability. This first study of the ice shelves is promising even though it is very complex to analysis. At this stage, it seems difficult to derive geophysical parameters of the ice shelf but more investigations are needed. Also in this case it is recognized as main problem the lack of in-situ data, which are essential to improve the model interpretation and analysis. Additional remote sensing data (high resolution, active/passive, optical and microwave) in combination with in-situ borehole data and ice shelve models will help to better understand the observed changes. The change maps can be used to identify specific regions of interest for future airborne field campaigns. e.g. on the Ronne-Filchner ice shelf. The dramatic changes observed over Larsen C and King George VI calls for immediate coordinated research action. A clear recommendation to explore the potential of a multi-sensor approach for the monitoring of ice shelves properties has been expressed during the recent ESA workshop (ESA Polar Science Collocation Meeting - 28-30 June 2017 ESA-ESRIN – report is in preparation)

Near-surface processes

The sensitivity of L-band T_B to snow surface properties has been highlighted for a specific event happening at Dome C on the Antarctic Plateau. The exceptional T_BH changes are linked to an exceptional hoar formation during the summer and possibly to significant snow accumulation. Both was made possible by weaker than normal wind for a long periods. The causes of the changes at the snow surface are complex and partially elucidated here. Useful information on changes in snow surface could be obtained for climatic studies, such as following trend at continent scale or

identifying specific event. This information is also important to better understand the heat exchanges that happen at the boundary layer between snow and atmosphere. Deeper analyses are needed in order to find the best way to retrieve useable information over the whole Antarctic ice sheet.

5 References

Abdalati W., and Steffen K., 1997, Snowmelt on the Greenland ice sheet as derived from passive microwave satellite data, J. of Climate, 10, 165-175, doi:10.1175/1520-0442(1997)010<0165:SOTGIS>2.0.CO;2.

Agosta C., Favier V., Krinner G., Gallée H., Fettweis X., and Genthon C., 2013, High-resolution modelling of the Antarctic surface mass balance, application for the twentieth, twenty first and twenty second centuries. Climate dynamics, 41(11-12), 3247-3260.

Al Bitar A., Mialon A., Kerr Y., Cabot F., Richaume P., Jacquette E., Quesney A., Mahmoodi A., Tarot S., Parrens M., Al-yaari A., Pellarin T., Rodriguez-Fernandez N., and Wigneron J.-P., 2017, The Global SMOS Level 3 daily soil moisture and brightness temperature maps. Earth System Science Data Discussions, doi:10.5194/essd-2017-1.

Bereiter B., Fischer H., Schwander J., and Stocker T. F., 2014, Diffusive equilibration of N2, O2 and CO2 mixing ratios in a 1.5 million years old ice core, The Cryosphere, 8(1), 245-256.

Brodzik M. J., Billingsley B., Haran T., Raup B., and Savoie M. H., 2012, EASE-grid 2.0: Incremental but Significant Improvements for Earth-Gridded Data Sets. ISPRS International Journal of Geo-Information, 1, 32-45. doi:10.3390/397 ijgi1010032.

Brogioni M., Macelloni G., Montomoli F., and Jezek K.C., 2015, Simulating Multifrequency Ground-Based Radiometric Measurements at Dome C, Antarctica. Selected Topics in Applied Earth Observations and Remote Sensing, IEEE Journal of, PP-99, 1-13, 10.1109/JSTARS.2015.2427512

Cook A. J. and Vaughan D.G., 2010, Overview of areal changes of the ice-shelves on the Antarctic Peninsula over the past 50 years, The Cryosphere, 4(1), 77-98.

Cuffey K.M. and W.S.B. Paterson, 2010, The physics of glaciers, Academic Press.

Dee D. P., Uppala S. M., Simmons A. J., Berrisford P., Poli P., Kobayashi S., et al., 2011, The ERA-Interim reanalysis: Configuration and performance of the data assimilation system. Quarterly Journal of the Royal Meteorological Society, 137(656), 553-597.

Fox Maule C., Purucker M. E., Olsen N., and Mosegaard K., 2005, Heat flux anomalies in Antarctica revealed by satellite magnetic data, Science, 309(5733), 464-467.

Fretwell P., Pritchard H. D., Vaughan D. G., Bamber J. L., Barrand N. E., Bell R., Bianchi C., Bingham R. G., Blankenship D. D., Casassa G., Catania G., Callens D., Conway H., Cook A. J., Corr H. F. J., Damaske D., Damm V., Ferraccioli F., Forsberg R., Fujita S., Gim Y., Gogineni P., Griggs J. A., Hindmarsh R. C. A.,

Holmlund P., Holt J. W., Jacobel R. W., Jenkins A., Jokat W., Jordan T., King E. C., Kohler J., Krabill W., Riger-Kusk M., Langley K. A., Leitchenkov G., Leuschen C., Luyendyk B. P., Matsuoka K., Mouginot J., Nitsche F. O., Nogi Y., Nost O. A., Popov S. V., Rignot E., Rippin D. M., Rivera A., Roberts J., Ross N., Siegert M. J., Smith A. M., Steinhage D., Studinger M., Sun B., Tinto B. K., Welch B. C., Wilson D., Young D. A., Xiangbin C., Zirizzotti A., 2013, Bedmap2: improved ice bed, surface and thickness datasets for Antarctica, The Cryosphere, 7, 375-393, doi:10.5194/tc-7-375-2013.

Fréville H., Brun E., Picard G., Tatarinova N., Arnaud L., Lanconelli C., and Van Den Broeke M., 2014, Using MODIS land surface temperatures and the Crocus snow model to understand the warm bias of ERA-Interim reanalyses at the surface in Antarctica. The Cryosphere, 8(4), 1361-1373.

Fricker H. A., Popov S., Allison I., and Young N., 2001, Distribution of marine ice beneath the Amery Ice Shelf, Geophysical Research Letters, 28, 2241–2244.

Hörhold M. W., Kipfstuhl S., Wilhelms F., Freitag J., and Frenzel A., 2011, The densification of layered polar firn, Journal of Geophysical Research: Earth Surface, 116(F1).

Jezek K. C., Johnson J. T., Drinkwater M. R., Macelloni G., Tsang L., Aksoy M., and Durand M., 2015, Radiometric Approach for Estimating Relative Changes in Intraglacier Average Temperature, IEEE Trans. on Geoscience and Remote Sensing, 53(1), 134-143.

Kaleschke L., Maaß N., Haas C., Hendricks S., Heygster G., and Tonboe R. T., 2010, A sea-ice thickness retrieval model for 1.4 GHz radiometry and application to airborne measurements over low salinity sea-ice,The Cryosphere, 4(4), 583-592.

Kaleschke L., Tian-Kunze X., Maaß N., Beitsch A., Wernecke A., Miernecki M., Müller G., Fock B., Gierisch A., Schlünzen K., Pohlmann T., Dobrynin M., Hendricks S., Asseng J., Gerdes R., Jochmann P., Reimer N., Holfort J., Melsheimer C., Heygster G., Spreen G., Gerland S., King J., Skou N., Søbjærg S., Haas C., Richter F., and Casal T., 2016, SMOS sea ice product: Operational application and validation in the Barents Sea marginal ice zone, Remote Sensing of Environment, 180, 264-273, doi:10.1016/j.rse.2016.03.009.

Kaleschke L., Tian-Kunze X., Maaß N., Mäkynen M., and Drusch M., 2012, Sea ice thickness retrieval from SMOS TB during the Arctic freeze-up period, Geophys. Res. Lett., 39, L05501, doi:10.1029/2012GL050916

Kerr Y. H., Jacquette E., Al Bitar A., Cabot F., Mialon A., Richaume P., Quesney A., and Berthon L., 2013, CATDS SMOS L3 soil moisture retrieval processor - Algorithm Theoretical Baseline Document (ATBD). Technical Report SO-TN-CBSA-GS-0029, Issue 2.e. URL: http://www.cesbio.ups-tlse.fr/SMOS_blog/wp-content/uploads/2013/08/ATBD_L3_rev2_draft.pdf.

Klein L., and Swift, C. T., 1977, An improved model for the dielectric constant of sea water at microwave frequencies. Antennas and Propagation, IEEE Transactions on, 25(1), 104-111.

Lambrecht A., Sandhger H., Vaughan D. G., and Mayer, C., 2007, New ice thickness maps of Filchner–Ronne Ice Shelf, Antarctica, with specific focus on grounding lines and marine ice, Antarctic Science, 19(04), 521-532.

Le Brocq A. M., A.J. Payne and A. Vieli, 2010, An improved Antarctic dataset for high resolution Geography numerical ice sheet models (ALBMAP v1), Earth Syst. Sci. Data, 2, 247-260, www.earth-syst-sci-data.net/2/247/2010/, doi:10.5194/essd-2-247-2010.

Leduc-Leballeur M., Picard G., Macelloni G., Arnaud L., Brogioni M., Mialon A., and Kerr Y., Influence of snow surface properties on L-band brightness temperature at Dome C, Antarctica. Remote Sensing of Environment, in revision.

Leduc-Leballeur M., Picard G., Mialon A., Arnaud L., Lefebvre E., Possenti P., and Kerr Y., 2015, Modeling L-Band Brightness Temperature at Dome C in Antarctica and Comparison With SMOS Observations. IEEE Trans. Geosci. Remote Sens., 53(7), 4022-4032.

Maaß, N., Kaleschke, L., Tian-Kunze, X., and Drusch, M., 2013, Snow thickness retrieval over thick Arctic sea ice using SMOS satellite data, The Cryosphere, 7, 1971–1989.

Macelloni G., Leduc-Leballeur M., Brogioni M., Ritz C., and Picard G., 2016, Analyzing and modeling the SMOS spatial variations in the East Antarctic Plateau, Remote Sensing of Environment, 180, 193-204, doi:10.1016/j.rse.2016.02.037.

Mätzler C., 2006, Thermal Microwave Radiation: Applications for Remote Sensing Chapter 5, Microwave dielectric properties of ice. Eds.

Mecklenburg S., Drusch M., Kaleschke L., Rodriguez-Fernandez N., Reul N., Kerr Y., et al, 2016, ESA's Soil Moisture and Ocean Salinity mission: From science to operational applications. Remote Sensing of Environment, 180, 3-18.

Nicholls K. W., 1996, Temperature variability beneath Ronne Ice Shelf, Antarctica, from thermistor cables, Journal of Geophysical Research: Oceans, 101, 1199–1210.

Nicholls K. W., 1997, Predicted reduction in basal melt rates of an Antarctic ice shelf in a warmer climate, Nature, 388, 460–462.

Nicholls K. W., and Jenkins A., 1993, Temperature and salinity beneath Ronne Ice Shelf, Antarctica, Journal of Geophysical Research: Oceans, 98, 22 553–22 568.

Nicholls K. W., Østerhus S., Makinson K., Gammelsrød T., and Fahrbach E., 2009, Ice-ocean processes over the continental shelf of the southern Weddell Sea, Antarctica: A review, Reviews of Geophysics, 47.

Nicholls, K. W., and Østerhus S., 2004, Interannual variability and ventilation timescales in the ocean cavity beneath Filchner-Ronne Ice Shelf, Antarctica, Journal of Geophysical Research: Oceans, 109.

Pattyn F., 2010, Antarctic subglacial conditions inferred from a hybrid ice sheet/ice stream model. Earth and Planetary Science Letters, 295(3), 451-461.

Picard G., and Fily M., 2006, Surface melting observations in Antarctica by microwave radiometers: correcting 26 year-long timeseries from changes in acquisition hours, Remote Sensing of Environment, 104(3), 325-336.

Purucker M., 2013, Geothermal heat flux data set based on low resolution observations collected by the CHAMP satellite between 2000 and 2010, and produced from the MF-6 model following the technique described in Fox Maule et al. (2005), available at: http://websrv.cs.umt.edu/isis/index.php

Rautiainen K., Lemmetyinen J., Pulliainen J., Vehviläinen J., Drusch M., Kontu A., Kainulainen J., and Seppänen J., 2012, L-Band radiometer observations of soil processes at boreal and sub-arctic environments, IEEE Trans. Geosci. Remote Sens., 50(5): 1483-1497.

Rautiainen K., Lemmetyinen J., Schwank M., Kontu A., Ménard C., Mätzler C., Drusch M., Wiesmann A., Ikonen J., and Pulliainen J., 2014, Detection of soil freezing from L-band passive microwave observations, Remote Sensing of Environment, 147, 206-218, doi:10.1016/j.rse.2014.03.007

Ridley J., 1993, Surface melting on Antarctic Peninsula ice shelves detected by passive microwave sensors. Geophys. Res. Lett., 20, 2639-2642. doi:10.1029/93GL02611.

Rignot E., Velicogna I., van den Broeke M. R., Monaghan A., and Lenaerts J. T. M., 2011, Acceleration of the contribution of the Greenland and Antarctic ice sheets to sea level rise, Geophys. Res. Lett., 38, L05503, doi:10.1029/2011GL046583.

Robin G. D. Q., 1955, Ice movement and temperature distribution in glaciers and ice sheets. Journal of Glaciology, 2(18), 523-532.

Scambos T. A., Bohlander J. A., Shuman C. A., Skvarca P., 2004, Glacier acceleration and thinning after ice-shelf collapse in the Larsen B embayment, Antarctica, Geophys. Res. Lett., 31, L18402.

Schwank M., Rautiainen K., Mätzler C., Stähli M., Lemmetyinenb J., Pulliainen J., Vehviläinen J., Kontub A., Ikonen J., Ménard C. B., Drusch M., Wiesmann A., and Wegmüller U., 2014, Emission of a snow-covered ground with focus on l-band, Remote Sensing of Environment, 154,180-191.

Schwank M., Stähli M., Wydler H., Leuenberger J., Mätzler C., and Flühler H., 2004, Microwave L-band emission of freezing soil, IEEE Trans. Geosci. Remote Sens., 42(6): 1252–1261.

Shapiro N. M., and Ritzwoller M. H., 2004, Inferring surface heat flux distributions guided by a global seismic model: particular application to Antarctica. Earth and Planetary Science Letters, 223(1), 213-224.

Skou N., Kristensen S. S., Søbjærg S. S., and Balling J., 2015, Airborne L-Band Radiometer Mapping of the Dome-C Area in Antarctica, IEEE J. Sel. Topics Appl. Earth Observ. and Remote Sens., 8(7), 3656-3664.

Steig E. J., Schneider D. P., Rutherford S. D., Mann M. E, Comiso J. C, and Shindell D. T., 2009, Warming of the Antarctic ice-sheet surface since the 1957 international geophysical year, Nature, 457, 459-462.

Tan S., Aksoy M., Brogioni M., Macelloni G., Durand M., Jezek K., Wang T., Tsang L., Johnson J., Drinkwater M., Brucker L., 2015, Physical Models of Layered Polar Firn Brightness Temperatures from 0.5GHz to 2GHz, IEEE Journal of Selected Topics in Applied Earth Observations and Remote Sensing.

Tian-Kunze X., Kaleschke L., Maaß N., Mäkynen M., Serra N., Drusch M., and Krumpen T, 2014, SMOS-derived thin sea ice thickness: algorithm baseline, product specifications and initial verification, The Cryosphere, 8, 997-1018, doi:10.5194/tc-8-997-2014.

Tiuri M. E., Sihvola A.H., Nyfors E., and Hallikaiken M., 1984, The complex dielectric constant of snow at microwave frequencies. IEEE J. of Oceanic Engineering, 9-5, 377-382, doi:10.1109/JOE.1984.1145645

Torinesi O., Fily M., and Genthon C., 2003, Interannual variability and trend of the Antarctic summer melting period from 20 years of spaceborne microwave data, J. of Climate, 16(7), 1047-1060.

Tsang L., Kong J. A., and Ding K.-H., 2000, Scattering of Electromagnetic Waves, Vol.1: Theories and Applications. Wiley Interscience.

Turner J., Lachlan-Cope T. A., Colwell S., Marshall G. J., and Connolley W. M., 2006, Significant warming of the Antarctic winter troposphere, Science, 311, 1914–1917.

Van de Berg W. J., Van den Broeke M. R., Reijmer C. H., and van Meijgaard E., 2006, Reassessment of the Antarctic Surface Mass Balance using Calibrated Output of a Regional Atmospheric Climate Model, J. Geophys. Res, 111, D11104, doi: 10.1029/2005JD006495

Van den Broeke M. R., 2008, Depth and Density of the Antarctic Firn Layer, Arc. Ant. Alp. Res., 40, 432–438.

Van den Broeke M. R., Van de Berg W. J., and Van Meijgaard E., 2006, Snowfall in Coastal West Antarctica much greater than previously assumed, Geophys. Res. Letters, 33, L02505, doi: 10.1029/2005GL025239

Van der Veen C.J., 2013, Fundamentals of Glacier Dynamics", CRC Press.

Van Liefferinge B. V., and Pattyn F., 2013, Using ice-flow models to evaluate potential sites of million year-old ice in Antarctica, Climate of the Past, 9(5), 2335-2345.

Vionnet, V., Brun, E., Morin, S., Boone, A., Faroux, S., Le Moigne, P., et al., 2012, The detailed snowpack scheme Crocus and its implementation in SURFEX v7. 2. Geoscientific Model Development, 5, 773-791.

West R. D., Winebrenner D. P., Tsang L., and Rott H., 1996, Microwave emission from density-stratified Antarctic firn at 6 cm wavelength, J. Glaciol., 42(140), 63–76.

Zhao T., Shi J., Bindlish R., Jackson T. J., Kerr Y. H., Cosh M. H., Cui Q., Li Y., Xiong C., and Che T., 2015, Refinement of SMOS multiangular brightness temperature toward soil moisture retrieval and its analysis over reference targets, IEEE Journal of Selected Topics in Applied Earth Observations and Remote Sensing, 8, 589–603.

Zwally H. J., and Fiegles S., 1994, Extent and duration of Antarctic surface melting, Journal of Glaciology, 40(136), 463-475.